A MEASUREMENT MODEL FOR PRECISION PULSAR TIMING

J. M. Cordes and R. M. Shannon

Astronomy Department, Cornell University, Ithaca, NY 14853
Draft version October 20, 2010

ABSTRACT

This paper describes a comprehensive measurement model for the error budget of pulse arrival times. Applications include forecasting timing errors for optimization of long-duration timing campaigns and identifying mitigation methods that can reduce the errors. The model takes into account many end-to-end effects from the neutron star to the telescope, with emphasis on plasma propagation effects (particularly interstellar scattering), which are stochastic in time and have diverse dependences on radio frequency. To reduce their contribution, timing measurements can be made over a range of frequencies that depends on a variety of pulsar and instrumentation-dependent factors that we identify. A salient trend for high signal-to-noise measurements of millisecond pulsars is that time-of-arrival precision is limited either by irreducible interstellar scattering or by pulse-phase jitter caused by variable emission within pulsar magnetospheres. Forecasts that ignore these contributions are likely to be overoptimistic. A cap on timing errors implies that pulsars must be confined to low dispersion measures and observed at high frequencies. Use of wider bandwidths that increase signal-to-noise ratios will degrade timing precision, after a point, if nondispersive chromatic effects are not mitigated. The allowable region in the dispersion measure-frequency plane depends on how chromatic timing perturbations are addressed in wideband measurements. Without mitigation, observations at 1.4 GHz or 5 GHz are restricted to DM $\lesssim$ 30 and $\lesssim$ 100 pc cm^{-3}, respectively. With aggressive mitigation of interstellar scattering and use of large telescopes to provide adequate sensitivity at high frequencies (e.g. Arecibo, FAST, phase 1 of the SKA, and the SKA), pulsars with DMs up to 500 pc cm^{-3} can be used in precision timing applications. We analyze several methods that involve wide-band fitting to arrival times at a given epoch prior to multi-epoch fitting. While the terms of greatest current astrophysical interest are achromatic (e.g. orbital and gravitational wave perturbations), their measurement may ultimately be limited by similarly achromatic stochasticity in a pulsar's spin rate.

1. INTRODUCTION

Timing of pulsars commenced with their original discovery over 40 years ago and has reaped enormous benefits in enabling fundamental tests of general relativity (Kramer et al. 2006), demonstrating the existence of gravitational waves (Taylor & Weisberg 1982), determining masses and other fundamental aspects of neutron stars (NSs) (Freire et al. 2009), and modeling of the interstellar medium (ISM) (Cordes et al. 1990; Ramachandran et al. 2006). The precision of time-of-arrival (TOA) measurements has improved progressively, allowing new areas of study to be targetted, such as higher-order relativistic corrections to orbits and the timing perturbation from low-frequency (nano-Hertz) gravitational waves (Detweiler 1979; Hellings & Downs 1983; Romani & Taylor 1983). The discovery of millisecond pulsars (MSPs) (Backer et al. 1982) opened the door to placing meaningful limits on or making detections of cosmological gravitational-wave (GW) backgrounds (Bertotti et al. 1983; Cordes & Stinebring 1984; Foster & Backer 1990; Stinebring et al. 1990; Kaspi et al. 1994). Projections based on improved timing methods and discovery of new MSPs now makes the detection of nano-Hz GWs plausible in the next decade (Cordes et al. 2004; Jenet et al. 2004; Kramer et al. 2004; Jenet et al. 2005a,b; Lee et al. 2008; Jenet et al. 2009; Hobbs et al. 2009; Verbiest et al. 2009; Hobbs et al. 2010).

This paper is motivated by the general goal of maximizing timing precision but especially for GW detection. The sensitivity of a pulsar-timing array (PTA) increases nonlinearly with data span length but likely requires 5 to 10 years to make detections of plausible GW backgrounds (Anholm et al. 2009; van Haasteren et al. 2009). The relevant GW frequencies are therefore in the $10^{-8} - 10^{-9}$ Hz range. Candidate signals include stochastic backgrounds from coalescences of supermassive black-hole binaries (Jaffe & Backer 2003; Sesana & Vecchio 2010) in galaxy mergers and from exotic sources, such as cosmic string interactions (Damour & Vilenkin 2005; Pshirkov & Tuntsov 2010). Precision timing has also been proposed as a means for detecting low-mass primordial black holes ($\lesssim 10^{-3}$ Earth masses) that make close flybys of the solar system (Seto & Cooray 2007). Individual GW sources may be detectable if they are sufficiently massive

and nearby (Finn & Lommen 2010). No matter the source, the targeted signals are very weak, requiring timing precisions along with stability of the pulsar clocks $\lesssim 100$ ns for a large number of MSPs over many years.

We present a measurement model that allows an end-to-end assessment of timing precision. We distinguish between phenomena that affect the time-tagging of pulses — TOA estimation — and the astrophysics of the pulsar clock. An illustration of this distinction consists of pulses that can be time-tagged to arbitrary precision, such as delta-function pulses with infinite signal-to-noise ratio, but where stochasticity in the pulsar spin rate and in interstellar delays introduces a random component into the arrival times. We thus separate terms in the timing equation that result from the quality of the astrophysical clock and over which we have no control (except by choice of pulsars) from those that can be mitigated through choices of observational parameters and by appropriate post processing. These include phase jitter intrinsic to the pulsar, instrumental effects, and all the strongly chromatic interstellar propagation effects. We acknowledge but do not analyze timing errors from instrumental polarization, time transfer, and solar system ephemerides, which are discussed in the literature and likely will be improved to the point of becoming secondary factors in timing precision.

Timing perturbations that are interstellar in origin are one of the main topics of this paper. Armstrong (1984) first pointed out that stochastic dispersion-measure variations could limit timing precision. A timing and interstellar scattering study (Cordes et al. 1990) of the MSP B1937+21 (J1939+2134), indicated that diffractive interstellar scintilltions (DISS) cause fast timing perturbations and that epoch dependent interstellar variations also occur. Diffractive TOA variations were also identified in observations and simulations by Coles et al. (2010). Foster & Cordes (1990) assessed the roles of dispersion measure and refraction-angle variations and concluded that non-dispersive interstellar effects need to be mitigated in precision timing programs. This was followed by a similar study by Hu et al. (1991). More recently, You et al. (2007) demonstrated the importance of correcting for dispersion measure variations in precision pulsar timing.

Our analysis leads to discussion of possible methods for removing most of the interstellar effects along with some of those intrinsic to the pulsar that affect TOA estimation. If measurements were made with the same telescope and the same intrumentation in a long timing program and that, hypothetically, the ISM caused chromatic perturbations that were epoch independent, much of the mitigation effort would be unnecessary. However, ISM effects *are* inherently stochastic and PTAs are expected to make use of multiple telescopes with instrumentation operating in different frequency bands that likely will change with time. Consequently mitigation of ISM effects must be done carefully.

Our studies also apply to cases where interstellar scattering limits the timing precision to milliseconds or worse, which is relevant to any pulsars in the Galactic center even when observed at frequencies above 10 GHz.

In a separate paper (Shannon & Cordes 2010, hereafter Paper I) we assess the role of spin noise in precision pulsar timing, which we mention here only briefly. A companion paper (Shannon & Cordes 2010, in preparation; hereafter Paper III) presents simulations that corroborate and probe more deeply the interstellar plasma effects we discuss here analytically. We defer to another paper a consolidated analysis of the requirements of a PTA for making detections of GWs.

In § 2 we summarize prominent physical contributions to arrival times. In § 3 we focus on achromatic and weakly chromatic timing perturbations. § 4 concentrates on strongly chromatic effects. In § 5 we consolidate various physical terms into a signal model for use in fitting arrival times. In § 6 we discuss the efficacy of different schemes for correcting arrival times for chromatic interstellar contributions. We summarize our conclusions in § 7. Appendices A and B present details of several contributions to arrival-time estimation errors. Appendix C considers the apparent frequency dependence of dispersion measures that results from scattering. Appendix D gives the details of a least-squares fitting formalism.

2. TERMS IN A PHYSICAL MODEL FOR PULSE PHASE

Timing equations have been presented (e.g. Backer & Hellings 1986; Edwards et al. 2006) that give a comprehensive inventory of deterministic contributions to the overall arrival time and, indeed, motivate timing studies in the first place. However, they have only incompletely addressed the timing error budget. Improvements in timing precision are always being strived for that allow new effects to be measured. We describe salient terms in the timing budget that must be considered in any precision timing analysis. We first categorize them in terms of their physical origin. Then we consolidate terms according to their statistical properties and wavelength dependence. Table 1 lists a comprehensive (but by no means exhaustive) set of terms and defines notation for deterministic and stochastic components. We designate the chromaticity of each effect, the spectral signature, and whether there is a correlation between different pulsar lines of

sight. Entries in Table 1 are labelled as astrophysical ('A' in column 2) if they determine the arrival time. Others are designated with 'T' if they contribute to TOA estimation errors. Some effects of course fall in both categories. Here we describe briefly some of the systematic astrophysical factors that determine the mean arrival time. A detailed discussion of interstellar perturbations is given in later sections.

Pulse phase is dominated by the spin rate of the NS and its deceleration by magnetospheric torques. The stochastic part includes glitches and timing noise, the latter typically showing low-freqency components with a red power spectrum and more rarely a bandpass spectrum (Hobbs et al. 2009, 2010). Timing noise may comprise torque pulses or step functions that arise from effects internal to the neutron star (superfluid-crust interaction) or within the magnetosphere. Recently Lyne et al. (2010) have shown that torque fluctuations in the form of jumps between discrete states at quasi-periodic intervals comprise much (but not all) of the timing noise in long-period pulsars. Spin fluctuations clearly are a nuisance for the use of pulsars as precision clocks, as is well known. The power spectrum for spin variations in some pulsars is degenerate or nearly so with that expected from some sources of cosmological GW backgrounds (Shannon & Cordes 2010), so unless timing noise can be removed, it will play a significant role in the choice of pulsars for PTAs. Lyne et al. (2010) show that distinct pulse shapes are correlated with the discrete torque states in some objects. The correlation must be close to unity to remove most of the timing noise and so far it is not clear that the correlation is large enough for timing noise to be ignorable in forecasts of timing precision.

Pulses emitted from the rotating magnetosphere are proxies for spin phase of the NS (with due allowance for any doppler shift from NS motion), but emission regions in the magnetosphere are not synchronized perfectly with the NS. Arrival times are (usually) calculated by fitting a template to pulse profiles obtained by averaging N pulses. Individual pulses are well known to vary in amplitude and pulse phase by large amounts, but by mechanisms that are not well understood. However they likely involve incomplete filling of the open-field line region in the magnetosphere by coherently radiating plasma (Ruderman & Sutherland 1975). Radio emission may occur at different altitudes in response to time variable pair plasma densities, which will change arrival times in accord with light-travel times, angular aberration, gravitational bending of ray paths, and any refraction in the magnetosphere (Barnard & Arons 1986). Arrival time perturbations from the finite number of pulses combined with intrinsic phase jitter imply that there is a correlation of TOA error with pulse shape. These changes in shape are much different in origin from those identified by Lyne et al. (2010) and signify changes in pulse phase rather than torque. Nonetheless, a sufficiently high correlation again implies another opportunity for correcting TOAs, which we explore elsewhere.

The evolution of pulse shapes with frequency includes changes in widths, separations and amplitudes of individual pulse components that comprise average profiles. Pulse widths typically scale with frequency as $W \propto \nu^{-x}$ with $x \lesssim 0.3$ (Mitra & Rankin 2002), so observations that strive for TOA precisions of 1% of the pulse width or better require mitigation of pulse shape changes. A key issue is the alignment of frequency-dependent profiles so that TOAs are consistent between frequencies. One prescription is to identify fiducial pulse phases at different frequencies so that the resulting TOAs match those expected from the cold-plasma dispersion law, $\propto \nu^{-2}$ (Craft 1970). This procedure will fail at the highest timing precisions because there are other frequency-dependent, interstellar time delays that scale differently with frequency (Romani et al. 1986; Cordes et al. 1986; Foster & Cordes 1990). A recent discussion of the interaction between pulse shape evolution with frequency and estimates of dispersion measures may be found in Ahuja et al. (2007). While the focus of this paper is on frequency-dependent plasma effects, a complete analysis must include *all* pulse shape changes.

Other entries in Table 1 correspond to deterministic contributions for orbital motion, gravitational lensing, and astrometric errors associated with referencing TOAs to the solar system barycenter (SSBC). Any error in the location of the SSBC from uncertainties in planetary perturbations or from passing sub-stellar objects (e.g. Seto & Cooray 2007) will produce a perturbation having a dipolar signature, which we designate as $\Delta t_{\mathrm{Newt,SSBC}}$. Stochastic perturbations from any orbital debris (R. Shannon et al., in preparation) and instrumental effects from time transfer and polarization calibration errors (e.g. Britton 2000; van Straten 2009) are included in the table.

While all listed phenomena must be confronted in precision timing programs, this paper focuses on those that affect estimation of individual TOAs, including pulse shape stability, additive noise, and especially delays that arise from dispersion, scattering and refraction in the interstellar plasma.

TABLE 1
SELECTED TIMING EFFECTS

Term	Type[a]	Mean Part		Stochastic Part		Achromatic or Chromatic[b]	Fluctuation Spectrum		PSR-PSR Correlation[d]	Comments
		Symbol	Value	Symbol	Value		Signature[c]	Shape		
Spin rate	A	$t_{\rm spin}$	yr	$\Delta t_{\rm spin}$	$\mu s - s$	a	B, R	$f^{-4} - f^{-6}$	U	
Magnetosphere:										
Pulse Shape	A, T	$t_{\rm P}$	$\mu s - ms$	—	—	c	—	—	U	$\nu^{-0.3}$
Pulse Jitter	A, T	—	—	$\Delta t_{\rm J}$	$< \mu s - ms$	c	W, B	see text	U	$\nu^{-0.3}$
Orbital	A	$t_{\rm orb}$	hr	$\Delta t_{\rm orb}$	$< ms$	a	L, R	$f^{-5/3}$	U	
Dispersion	A, T	$t_{\rm DM}$	$\lesssim s$	$\Delta t_{\rm DM}$	$\lesssim 100\mu s$	C	R	$f^{-5/3}$	U	ν^{-2}
Faraday Rotation	A, T	$t_{\rm RM}$	$\lesssim \mu s$	$\Delta t_{\rm RM}$	$\lesssim ns$	C	R	$f^{-5/3}$	U	ν^{-3}
Interstellar Turbulence										
Pulse Broadening	A, T	$t_{\rm PBF}$	$ns - s$	$\Delta t_{\rm PBF}$	$< ns - ms$	C	—	complex	U	$\nu^{-4.4}$
DISS	A, T	—	—	$\Delta t_{\delta \rm PBF}$	$\lesssim \mu s$	C	W	flat	U	$\nu^{-1.6} - \nu^{-4.4}$
RISS	A, T	$t_{\rm PBF,RISS}$	$\lesssim \mu s$	$\Delta t_{\delta \rm PBF,RISS}$	$\lesssim \mu s$	C	R	$f^{-7/3}$	U	?
Angle of Arrival	A, T	—	—	$\Delta t_{\rm AOA}$	$\lesssim \mu s$	C	R	$f^{-2/3}$	U	ν^{-4}
Angle of Arrival	A, T	—	—	$\Delta t_{\rm AOA,SSBC}$	$\lesssim \mu s$	C	R	$f^{-1/3}$	U	ν^{-2}
Multipath averaging	A, T	—	—	$\Delta t_{\rm DM,\nu}$	$\lesssim 0.1\mu s$	C	R	complex	U	$\nu^{-23/6}$
Astrometric[e]	T	$t_{\rm AST}$		$\Delta t_{\rm AST}$		a	—	—	U	
Newtonian solar perturbations	T	—	—	$\Delta t_{\rm Newt,SSBC}$		a	—	—	C	dipolar
Radiometer Noise	T	—	—	$\Delta t_{\rm S/N}$	$< \mu s - ms$	c$\rightarrow$C	W	flat	U	$\nu^{0} \rightarrow \nu^{-2.7}$
Polarization	T	—		$\Delta t_{\rm pol}$		c	W	flat	U	
Gravitational Lensing	A	$t_{\rm GL}$		$\Delta t_{\rm GL}$		a	—	—	U	Episodic
Cosmic Strings	A	$t_{\rm STR}$		—		a	R	$f^{-16/3}$	U	Red noise if multiple events
Gravitational Waves	A	—	—	$\Delta t_{\rm GW}$	$\lesssim 100$ ns	a	R	$f^{-13/3}$	C, U	Two terms

[a] A = astrophysical, T = timing estimation error

[b] a = achromatic, C = strongly chromatic, c = weakly chromatic

[c] Fluctuation spectrum properties: R = red, W = white, B = bandpass, L = lowpass

[d] U = uncorrelated between different pulsar lines of sight, C = correlated

[e] Includes clock errors and Earth spin variations

Cordes & Shannon

3. ACHROMATIC AND WEAKLY CHROMATIC TOA PERTURBATIONS

The consolidated stochastic and achromatic term (including weakly chromatic contributions listed in Table 1) is

$$\Delta t_{S,A} = \Delta t_{J} + \Delta t_{AST} + \Delta t_{S/N} + \Delta t_{pol}. \tag{1}$$

In the following we are most interested in terms that appear even when astrometric contributions and instrumental polarization are dealt with perfectly.

Assuming that astrometric and polarimetric errors are negligible after appropriate processing, a simplified stochastic, achromatic term that includes only pulse phase jitter and radiometer noise, is

$$\Delta t_{S,A} = \Delta t_{J} + \Delta t_{S/N}. \tag{2}$$

Both terms affect the shape of the pulse profile formed from a finite number of pulses and thus contribute to the random error in the arrival time.

3.1. *Radiometer Noise*

Radiometer noise adds to the pulse shape measured in any of the Stokes parameters. The resulting TOA error standard template fitting (Downs & Reichley 1983) is approximately $W/$SNR, where W is the pulse width and SNR is the signal to noise ratio of the pulse. The frequency dependence of the sky background is strong ($T_{sky} \propto \nu^{-2.7}$) at frequencies below about 0.5 GHz. However, for higher frequencies usually used for precision timing, the frequency dependence is weaker. The signal-to-noise ratio involves the pulsar's radio spectrum that typically also declines with frequency, canceling much of the variation of the sky brightness temperature with frequency. We designate radiometer noise as weakly chromatic in Table 1 and bundle it with stochastic achromatic terms. In some cases, however, the pulsar's spectrum is flat (Lorimer et al. 1995), so the signal-to-noise ratio can be strongly chromatic.

In Appendix A we derive the *minimum* TOA error that applies when the conditions for matched filtering are satisfied, namely that the measured pulse shape comprises an invariant templae shape added to noise; our analysis assumes that the noise is white. For a sum of $N = 10^6 N_6$ pulses, is

$$\Delta t_{S/N} = 1 \ \mu s W_{ms} N_6^{-1/2} SNR_1^{-1} (\Delta/W)^{1/2} = 0.71 \ \mu s \ (\nu/1.4 \ \text{GHz})^{-\alpha_p} P_{ms}^{-1} W_{ms}^{3/2} (B \, N_6)^{-1/2} (S_{sys}/S_{1400}). \tag{3}$$

In the first form, SNR_1 is the signal-to-noise ratio of a single pulse (defined as the ratio of pulse peak amplitude to rms noise) and W is the effective pulse width defined in Appendix A, expressed here with a fiducial value of 1 ms. For a Gaussian pulse shape the effective width is $W = W_{FWHM}/\sqrt{2\pi \ln 2} \approx 0.69 W_{FWHM}$. The quantity Δ is approximately equal to the time resolution. In the second form, which shows explicitly that $\Delta t_{S/N}$ is independent of Δ, S_{sys} is the system temperature expressed in Jy; S_{1400} and α_p are the period-averaged flux density in mJy and the spectral index, respectively; the radio frequency ν and bandwidth B are in GHz; and the spin period P is in ms.

The appropriate values for pulse width W and SNR_1 include any distortions that broaden the pulse and reduce its amplitude. Residual dispersion smearing is one such effect, although it is negligible if pulses are coherently dedispersed. Broadening from interstellar scattering of distant pulsars observed at low frequencies makes the pulse asymmetric and thus non-Gaussian, so the expression is only approximately correct.

Another way that the ISM affects the timing error is through DISS of low-DM pulsars observed at high frequencies, which can cause the apparent flux density to be much smaller or much larger than average. TOAs are sometimes obtained only during scintillation maxima (e.g. Hotan et al. 2006) which can enhance the SNR by two orders of magnitude, reducing the noise-induced error below other contributions.

3.2. *Pulse Jitter and Amplitude Modulations in Known Pulsars*

All well-studied canonical pulsars (CPs) show phase jitter and amplitude modulations like that in Figure 4 of McLaughlin et al. (2002). Individual pulse amplitudes vary by 100% (or more) and pulse phases jump by of order the single-pulse width. Empirically, the average pulse shape of a pulsar is as much determined by the PDF of the phase jitter as it is by the shapes of individual pulses, a description first made by Craft (1970). The commonly-used intensity modulation index m_I (the rms intensity divided by the mean as a function of pulse phase), is typically of order unity and quantifies both the amplitude modulation and the phase jitter. Phase jitter appears to be statistically independent between pulses in some objects, while others show systematic drifts over several to many pulse periods, yielding an effective number of independent pulses $N_i \leq N$ in an N-pulse average. We distinguish jitter from sustained "mode" changes in pulse shape displayed by some pulsars, where pulse shapes switch between two or three preferred shapes. We quantify

phase jitter alone; if mode changes are unaccounted for in TOA estimates, they will only exacerbate the timing estimation error. We use the dimensionless quantity f_J to quantify the rms phase jitter in terms of the intrinsic pulse width, W_i.

Objects other than CPs also show phase jitter. The Crab pulsar shows giant pulses with amplitudes several hundred times larger than the mean pulse amplitude; giant pulses are intrinically narrow $(1 - 10\ \mu s)$ but show TOA jitter $\sim 100\ \mu s$ (Lundgren et al. 1995; Sallmen et al. 1999; Cordes et al. 2004). Giant pulses from the MSP B1937+21 show $f_J \approx 0.2 - 0.5$ (Kinkhabwala & Thorsett 2000). However, in stark contrast, the ordinary (non-giant) pulses from this pulsar apparently show negligible jitter (Jenet et al. 2001; Jenet & Gil 2004). Other MSPs show jitter similar to that of CPs, including J0437-4715, the brightest known MSP (Jenet et al. 1998). Edwards & Stappers (2003) show that the autocorrelation function (ACF) of the average profile for the recycled 41-ms pulsar J1518+4904 is about twice the width of the ACF of single pulses (their figure 9), an effect that can be accounted for only with phase jitter.

Jitter is related to pulse-shape stability that has been quantified using the cross correlation coefficient $\rho(N)$ between a template profile and sub-averages of N pulses (Helfand et al. 1975; Rathnasree & Rankin 1995). These analyses typically show $1 - \rho$ declining as N^{-1} for some ranges of N (as expected for statistically independent phase jitter between pulses) while in some objects the trend is flatter for small N, signifying correlations between pulses. It can be shown that the correlation coefficient is

$$\rho(N = 1) = \left[(1 + m_I^2)(W_U/W_a)\right]^{1/2} = \left(1 - f_J^2\right)^{1/4} / \left(1 + m_I^2\right)^{1/2}, \tag{4}$$

where W_U is the characteristic width of the template profile, W_a is the characteristic width of an individual pulse and we have used the relation, $f_J^2 = 1 - W_a^2/W_U^2$. Typically with $m_a = 1$ and $W_U = 2W_a$, we expect $\rho(N = 1) = 1/2$. For large N we have $\rho(N) \approx 1 - (1/2N)(1 + m_a^2)(W_U/W_a)$. Correlation values reported in previous stability analyses are consistent with these estimates, indicating that $f_J \sim 1/3$ to $1/2$ for most pulsars.

3.3. *Timing Error from Pulse-phase Jitter*

When TOAs are calculated from averages of N pulses, any given profile will depart stochastically from a long-term average, even when the SNR is large. Template fitting therefore yields a jitter-induced error that adds quadratically to the minimum expected from matched filtering. The role of jitter in pulse-shape stability and timing has been discussed in the past (Cordes & Downs 1985; D'Alessandro et al. 1993; Cordes 1993), but little overall attention has been given to its role in precision timing.

The TOA error $\propto W_i/\sqrt{N}$ is pulsar dependent. (Appendix A). Because single pulses from many pulsars appear to be broadband with modest frequency dependence, the jitter timing perturbation in a typical data set is only slightly dependent on frequency and can be viewed as a stochastic element of the systematic profile evolution in frequency described earlier. For simplicity, in some of our analysis we will consider the jitter effect to be stochastic in time but constant in frequency. For Gaussian-shaped pulses and a Gaussian probability density function (PDF) for pulse phase jitter,

$$\Delta t_J = 0.28 \mu s\, W_{i,\mathrm{ms}} N_6^{-1/2} \left(\frac{f_J}{1/3}\right) \left(\frac{1 + m_I^2}{2}\right)^{1/2}. \tag{5}$$

Figure 1 shows the rms TOA error caused by different levels of phase jitter from simulations. The left-hand panel shows a sequence of pulses that displays pulse-phase jitter with $f_J = 1/3$. The right-hand panel shows the rms arrival-time error for pulse profiles formed from a fixed number of single pulses (10^3) as a function of signal to noise ratio and for different values of f_J. For $f_J = 1/3$, the rms error is double that from additive noise once the single-pulse SNR exceeds a few tenths, which is consistent with a comparison of Eq. 3, 5.

In Figure 2 we show a jitter analysis for the MSP J1713+0747. Data were obtained at the Arecibo Observatory at 1.38 GHz using a baseband recording system, coherently dedispersed to yield high-time-resolution, and averaged synchronously using a timing model from P. Demorest and D. Nice (Demorest 2007, private communication). Details of the data acquisition and other analyses will be described elsewhere (Shannon et al., in preparation). We compare TOA errors expected from radiometer noise alone to those actually measured. First we take a high S/N template profile, add white noise, and then calculate the arrival time. Repeating over a large number of realizations and for different amounts of noise yields the open circles shown in Figure 2. We use Eq. 3 and calculate the effective width using the template profile and Eq. A2. The numerical rms TOA error agrees very well with the predicted error. Actual data show excess TOA variations. We calculated TOAs for an initial set of 10-s averages (2188 pulse periods) and then for 20-s, 40-s averages, etc. A jitter parameter, estimated assuming $m_I = 1$,

$$f_J = \left[N \left(\sigma_{\mathrm{TOA}}^2(N) - \sigma_{\mathrm{TF}}(N)^2\right) / \left(1 + m_I^2\right)\right]^{1/2} \approx 0.4 \tag{6}$$
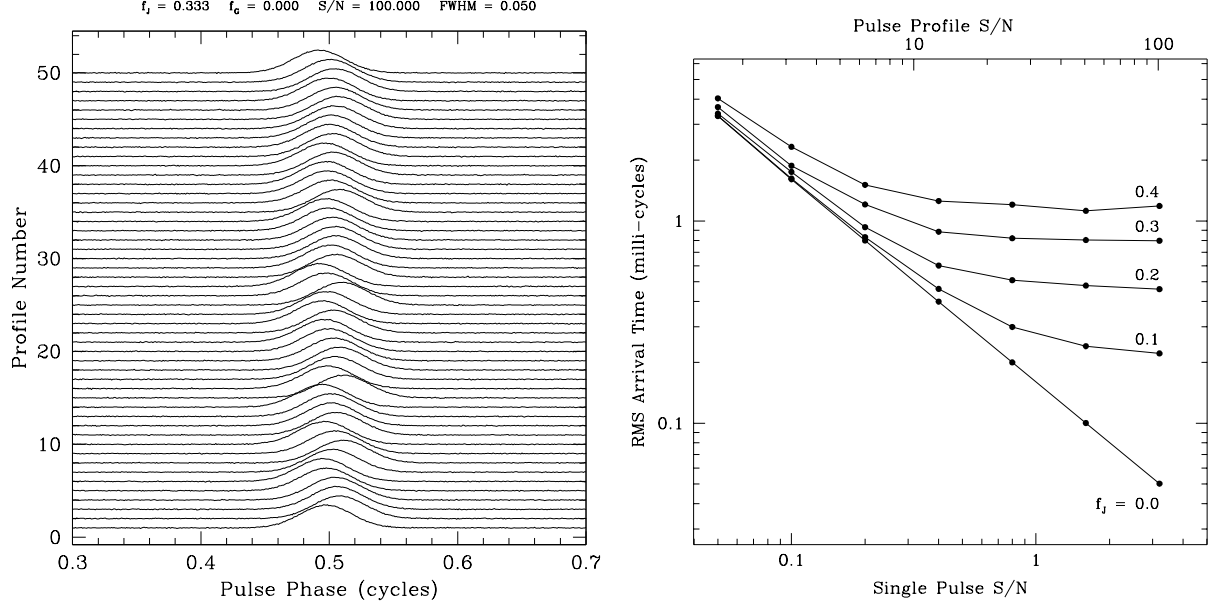
Fig. 1.— (Left) Simulated pulse sequence of showing pulse phase jitter with $f_J = 1/3$ and a unity intensity modulation index. The net duty cycle is 0.05. (Right) Arrival time error vs signal to noise ratio (SNR) for simulated data with different amounts of pulse phase jitter, as labelled. TOAs were calculated from averages of 10^3 pulses to yield a SNR for each profile that is $10^{3/2}$ larger than the single-pulse SNR. Each plotted point is based on 500 realizations.

accounts for the excess timing error over that expected from template fitting (TF) to a profile consisting of the template combined with additive noise to yield the same SNR as the real data.
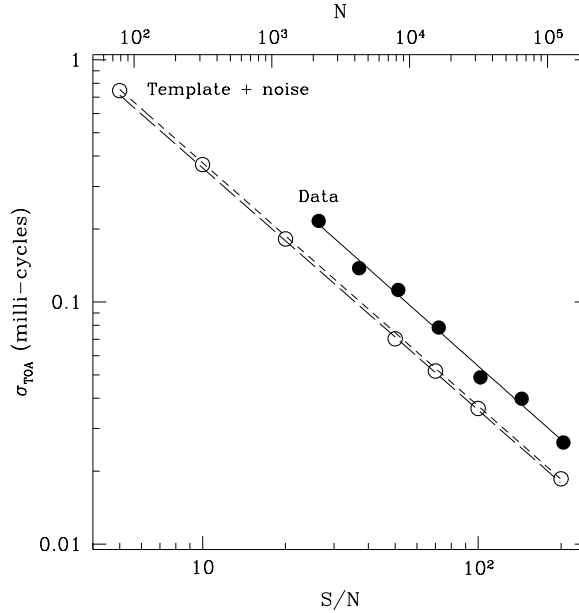

Fig. 2.— Arrival time analysis for the MSP J1713+0747 at 1.4 GHz. The points are calculated for pulse profiles calculated from different numbers of pulses (N, top axis) yielding increasing signal-to-noise ratios (bottom axis). The lower set of points results from calculating TOAs from simulated data formed by adding a high SNR template to gaussian noise. The upper set of points is from fits to actual data obtained with different integration times. The short-dashed curve is the fit to the points. The long-dashed curve is the prediction using Eq. A1-A2, which assumes that data comprise identical pulse shapes with additive noise. The two curves are actually coincident but have been displaced by ±0.01 in the log for clarity. The actual data have higher TOA errors than simulated values because pulse-phase jitter causes pulse shapes to differ from the template shape. A jitter parameter $f_J \approx 0.4$ accounts for the difference.

3.4. *Jitter vs Noise Dominated Timing Errors*

We compare jitter and noise contributions to the TOA error for the known sample of pulsars by using cataloged parameters (Manchester et al. 2005) and assuming reasonable values for amplitude modulation ($m_I = 1$) and phase jitter ($f_J = 1/3$). Figure 3 gives the fraction of MSPs for which phase jitter dominates the radiometer noise error. We assume that jitter is statistically independent between pulses so that $N_i = N$, which may *underestimate* the TOA error. Fractions are calculated by counting objects for which $\Delta t_J > \Delta t_{S/N}$ for different system temperatures (in flux-density units, Janskys) that correspond to 100-m class telescopes (e.g. the Effelsberg and Green Bank Telescopes, the Expanded VLA, and the Parkes and Sardinia telescopes), Arecibo-class telescopes (Arecibo itself, the Chinese FAST telescope, and Phase 1 of the Square Kilometer Array, SKA), and Phase 2 of the SKA, which is projected to have $S_{\rm sys}$ of order ten times smaller than for Phase 1. Results are shown for frequencies from 0.3 to 5 GHz using either the cataloged spectral index of the pulsar's flux density or using a power law $\propto \nu^{-2.0}$.

The results indicate that usage of more sensitive telescopes (whether by larger collecting area, lower system noise, or greater bandwidths) will lead to timing measurements that are limited by phase jitter. To increase the timing precision, the only recourse is to make use of longer integration times per TOA. It may also be possible to reduce the timing error from phase jitter if the resulting pulse shape variations are correlated with the timing error. A method based on principal component analysis will be reported separately (Cordes et al., in preparation).
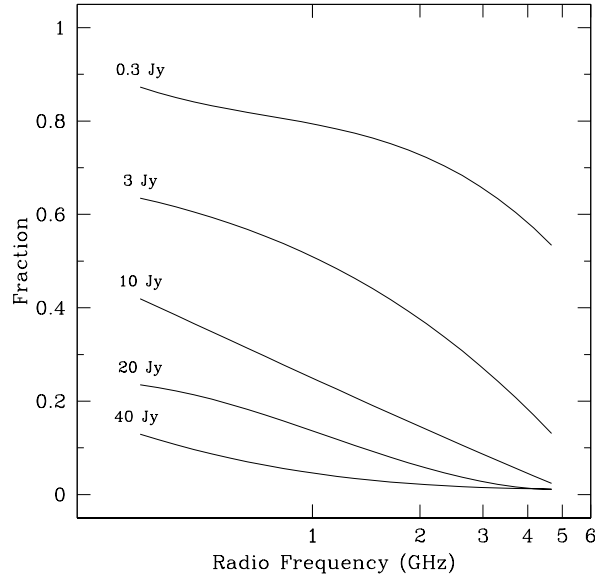

FIG. 3.— Fraction of known pulsars with jitter timing error larger than that from radiometer noise, i.e. $\Delta t_J > \Delta t_{S/N}$. The curves are labeled by the system equivalent flux density, $S_{\rm sys}$, at 1.4 GHz. $S_{\rm sys}$ varies with frequency by adding the Galactic synchrotron contribution as 20 K $(\nu/0.408 \; {\rm GHz})^{-2.75}$ as quantified by Cortés (2007). Calculations were done with 10% bandwidths below 1 GHz and bandwidths of 0.4 and 0.8 GHz at 1.4 and 2 GHz, and 1 GHz bandwidths at 3 GHz and higher. Each MSP with $P < 20$ ms that had tabulated flux densities in the pulsar catalog of Manchester et al. (2005) is included. Given that only 82 MSPs in the current catalog satisfy the criteria, a cubic fit was done to the computed fraction to plot each curve.

4. STRONGLY CHROMATIC TOA PERTURBATIONS

Stochastic and strongly chromatic timing perturbations include contributions from plasma dispersion, Faraday rotation and interstellar scattering (ISS),

$$\Delta t_{S,C} = \Delta t_{\rm DM} + \Delta t_{\rm RM} + \Delta t_{\rm ISS}. \tag{7}$$

The dispersion term receives contributions from the ionosphere, interplanetary medium (IPM), and the ISM. Any extragalactic pulsars will also involve the intergalactic medium and the ISM of their host galaxy. The ISS term comprises six separate terms

$$\Delta t_{\rm ISS} = \Delta t_{\rm PBF} + \Delta t_{\rm AOA} + \Delta t_{\rm AOA,SSBC} + \Delta t_{\delta \rm PBF} + \Delta t_{\delta \rm PBF,RISS} + \Delta t_{\rm DM,\nu}. \tag{8}$$

These are respectively the delay associated with diffractive pulse broadening, the delay from angle-of-arrival (AOA) variations, the error in referencing TOAs to the SSBC due to AOA variations, the error from fast variations in the pulse-broadening function (PBF) that describes diffractive pulse broadening, slow variations in the PBF induced by refraction, and the perturbation of DM that results from averaging over the scattering cone. We discuss these terms in detail in § 4.3.

The relative amplitudes of ISS effects depend on the spatial properties of the ISM. The standard approach is to characterize small-scale variations in electron density ($\lesssim 1000$ AU) — those that diffract and refract radiation from point sources — with a wavenumber spectrum and to consider large-scale variations (e.g. cloud-like, sheet-like and filamentary structures) as modulations of the spectrum. Small scale variations largely appear to be consistent with a Kolmogorov spectrum and in many cases the variations involve anisotropic irregularities with large axial ratios (Cordes et al. 2006; Brisken et al. 2010). Regardless of the detailed shape of the wavenumber spectrum, so long as it is broad, three regimes of scattering can be defined (Rickett 1990; Cordes & Lazio 1991). When the phase perturbation by the scattering medium is much smaller than a radian across one Fresnel scale $\sim \sqrt{\lambda D_{\mathrm{eff}}}$, where λ is the wavelength and D_{eff} is a characteristic distance, a point-source will appear largely as a point source with a small halo around it. When the phase perturbation is large, the scattering is strong. All of the source flux will be scattered and the scintillation bandwidth $\Delta\nu_d \ll \nu$. So long as the scattering length $\ell_d = \lambda/\theta_d$ is larger than any minimum (inner) scale ℓ_i in the wavenumber spectrum, the scaling of $\Delta\nu_d$ with ν is a function of the spectrum's slope (if shallow enough). For super-strong scattering, $\ell_d < \ell_1$ and the scaling laws generally will be different than in the strong-scattering regime. In particular, they will conform to a medium with a square-law phase structure function. Electron density fluctuations appear to exist on a wide range of scales from $\sim 10^3$ km to Galactic scales so, accordingly, there is a large range of expected time scales (Armstrong et al. 1995).

When scattering is weak, only a fraction of the pulsar's flux is scattered, the remainder appearing as a point source. In this case, the delay of the pulse is negligible because even the scattered portion is delayed by only $(2\pi\nu)^{-1} \approx 0.1$ ns. The transition from weak to strong scattering occurs approximately when $\Delta\nu_d/\nu = 1$ or $\nu_{\mathrm{trans}} = C_1/(2\pi\overline{\tau}_d)$. Using $\tau_d = \tau_{d0}\nu^{-4.4}$, the broadening time at 1 GHz and with ν in GHz, (the Kolmogorov scaling when there is neglibile inner scale), we obtain $\nu_{\mathrm{trans}} = (2\pi\tau_{d0}/C_1)^{0.29} = 12.1$ GHz $\tau_{d0}(\mu s)^{0.29}$. From Figure 4, which shows values of τ_d at 1 GHz plotted against DM, the transition frequency is about 2.3, 12 and 24 GHz for pulsars with DMs of 10, 50 and 100 pc cm^{-3}.

4.1. *Dispersion Measure Variations*

For a total DM from all contributions along the line of sight (LOS), the group delay is

$$t_{\mathrm{DM}} = a_{\mathrm{DM}} \mathrm{DM} \, \nu^{-2} \tag{9}$$

where $a_{\mathrm{DM}} = 4.15$ ms for DM in standard units of pc cm^{-3}. Fluctuations δDM(t) affect the arrival time itself and, if large enough and unaccounted for, can distort the pulse shape and affect the TOA. In the following we ignore such distortion because it is addressible in the data processing. DM variations produced by structure in the ISM are stochastic in time but deterministic in frequency (however, see § 4.4). Measured variations are seen on a variety of time scales that are consistent with a broad spectrum of electron-density variations in the ISM (Armstrong 1984; Cordes et al. 1990; Rickett 1990; Phillips & Wolszczan 1991; Backer et al. 1993; Kaspi et al. 1994; Cognard & Lestrade 1997). Amplitudes depend on the distance and velocity of the pulsar but maximum rates of change $\sim 10^{-3}$ pc cm^{-3} per year. The temporal fluctuation spectrum for DM has the same form as the electron-density spectrum (Armstrong 1984) and has large fluctuations on longer time scales. During a typical observing session at a given epoch (e.g. $\lesssim 1$ hr), DM variations are too small to be detected with known pulsars. As is well known, however, precision timing requires removal of DM variations between epochs (e.g. You et al. 2007).

The precision needed for DM is stringent. The simplest case is when the only other TOA perturbation is from white-noise measurement error. We write the TOA as the sum of achromatic, dispersive, and white-noise terms:

$$t_\nu = t_\infty + t_{\mathrm{DM}}(\nu) + t_{\mathrm{W}}(\nu), \tag{10}$$

where t_∞ is the achromatic arrival time at infinite frequency (which would include spin noise and gravitational wave contributions). Here we ignore any frequency dependent profile "evolution" intrinsic to the pulsar. For a two-parameter (t_∞ and DM) least-squares fit across a frequency range $[\nu_2, \nu_1]$ sampled in n_ν channels, the error on the achromatic TOA is $\sigma_{t_\infty}^2 = s_4/(s_0 s_4 - s_2^2)$, where s_p is a weighted sum over frequencies defined in Eq. D1. For equal errors in all channels σ_{t_∞} depends only on the frequency ratio $r = \nu_1/\nu_2 > 1$, as expected. An alternative method would use a value for DM obtained from ancillary,

non-contemporaneous measurements to correct TOAs rather than fitting for DM from the TOAs. For this procedure to be at least as good as fitting for DM, the error in δDM must satisfy

$$\delta\text{DM} < 10^{-3.38} \text{ pc cm}^{-3} \frac{\nu_1^3}{B}(1 - B/\nu_1)^{3/2}\sigma_B(\mu s) \tag{11}$$

for ν_1 and $B = \nu_1 - \nu_2$ in GHz and a fiducial radiometer noise TOA error $\sigma_B = 1$ μs (c.f. Eq. 3). In this expression, we assume that errors are independent of frequency and emphasize that this is just the radiometer noise contribution to the error.

Measured DM changes are at levels expected for interstellar electron-density variations that have a power-law wavenumber spectrum. For a power-law spectrum $C_n^2 \times (\text{wavenumber})^{-\beta}$, where C_n^2 is simply a spectral coefficient in the wavenumber spectrum, the structure function for DM has an ensemble average, denoted by angular brackets (e.g. Cordes & Rickett 1998; You et al. 2007),

$$D_{\text{DM}}(\tau) = \left\langle [DM(t) - DM(t + \tau)]^2 \right\rangle = f_\alpha \int_0^D ds \, |\mathbf{V}_{\text{eff}\perp}(s)|^\alpha C_n^2(s) \approx \frac{f_\alpha}{\alpha + 1}\text{SM}\,(\tau V_p)^\alpha, \tag{12}$$

where $\alpha = \beta - 2$, f_α is a constant, $\mathbf{V}_{\text{eff}\perp}$ is an effective velocity, and SM, the scattering measure, is the LOS integral of C_n^2. The approximate equality holds for constant C_n^2 and when the pulsar transverse velocity dominates the effective velocity $V_{\text{eff}\perp}$. For a Kolmogorov medium, $f_{5/3} = 88.3$, and using standard units for scattering measure (kpc m$^{-20/3}$), the rms difference in DM between two epochs separated by τ (in years) is

$$\sigma_{\text{DM}}(\tau) = [(1/2)D_{\text{DM}}(\tau)]^{1/2} \approx 10^{-3.47} \text{ pc cm}^{-3} \left(\text{SM}/10^{-3.5} \text{ kpc m}^{-20/3}\right)^{1/2} \left(\tau_{\text{yr}}V_{\text{P}100}\right)^{5/6} \tag{13}$$

for pulsar velocity in units of 100 km s^{-1}. This rms is comparable to measured changes in DM for nearby pulsars that have SM $\approx 10^{-3.5}$ kpc m$^{-20/3}$. From Eq. 13 and 11 if we require a timing error less than 0.1 μs for $3\sigma_{\text{DM}}(\tau)$, then the DM and TOA measurements need to be made within $\tau < 8$ days. This result is in accord with those determined numerically in Paper III.

4.2. *Profile Splitting from Faraday Rotation*

The TOA perturbation from a magnetized plasma includes a birefringent term that is equal and opposite for the two hands of circular polarization, $t_{\text{RM}} = \pm 0.18$ ns ν^{-3}RM for RM in standard units of rad m^{-2}. The empirical manifestation is *profile splitting* of the two polarizations. For the extreme case of high-RM pulsars observed at low frequencies, the profile splitting produces a pseudo-circular polarization that would cause a sign-changing Stokes parameter $V = I_L - I_R$ even when the circular polarization intrinsic to the pulsar is zero. If uncorrected, the total intensity profile $I = I_L + I_R$ is broadened slightly but symmetrically relative to the true TOA, so the TOA error is not biased one way or another. Correction of this effect, if ever necessary, needs to be done prior to summing the two hands of polarization and can be incorporated into the coherent dedispersion process. Values of RM for Galactic lines of sight can range up to 10^3 rad m^{-2} but for objects within 1 kpc, typical RMs are a few tens of rad m^{-2} or less. The RM perturbation is therefore negligible compared to a 100-ns timing error unless distant pulsars with large RMs are observed at low frequencies.

4.3. *Interstellar Scattering and Refraction*

The interstellar timing perturbations in Eq. 8 result from refraction and multipath propagation caused by scattering from small-scale electron-density variations. The resulting timing perturbations have distinct time-frequency characteristics:

1. Variations in dispersion measure from frequency-dependent spatial averaging of the phase perturbation ($\Delta t_{\text{DM},\nu}$);
2. The mean time delay associated with multipath broadening of pulses from diffraction (Δt_{PBF});
3. Fast, stochastic changes in the diffractive delay associated with the finite number of "scintles" in the sampled time-frequency plane ($\Delta t_{\delta\text{PBF}}$);
4. A time delay associated with the stochastic refraction angle of arrival (AOA, Δt_{AOA});
5. An AOA induced error associated with transforming measured TOAs to the SSBC ($\Delta t_{\text{AOA,SSBC}}$), which arises from the difference between the assumed and actual direction to the pulsar; and
6. Modulations of the mean time delay from wavefront curvature induced by large-scale variations, which also causes refractive interstellar scintillation (RISS; $\Delta t_{\delta\text{PBF,RISS}}$).

The first effect is the modification of DM by the frequency-dependent spatial averaging of the electron-density along different propagation paths. The second (typically dominant) effect is the delay introduced by the pulse broadening function (PBF) that is convolved with the true pulse shape. The PBF is causal, so the delay is always positive. It is also strongly frequency dependent. The PBF is stochastic from refractive variations and from the scintillation fluctuations contained in the finite bandwidth and integration time used to form a pulse profile. The angle of arrival (AOA) of the centroid of the bundle of multipath "rays" varies from refraction in the ISM and adds another frequency-dependent delay with a different frequency dependence. Finally, the AOA induces an error in the correction of topocentric TOAs to the SSBC (Foster & Cordes 1990).

We characterize the second and last three effects as a mean delay that changes slowly with time (hours to years). The third effect differs from the others because it involves interstellar diffraction features that are statistically independent between data sets used to calculate individual TOAs. We give a detailed analysis in the next section.

For a Kolmogorov medium in the strong-scattering regime, refraction angles are much smaller than diffraction angles, so the TOA perturbations included in Eq. 8 may be ordered as

$$\Delta t_{\text{DM},\nu} \lesssim \Delta t_{\text{AOA}} \lesssim \Delta t_{\text{AOA,SSBC}} \lesssim \Delta t_{\delta\text{PBF,RISS}} \lesssim \Delta t_{\delta\text{PBF}} \lesssim \Delta t_{\text{PBF}} \tag{14}$$

because the two smallest terms depend quadratically and linearly on the refraction angle, θ_r, while the other terms depend on powers of the diffraction angle, θ_d. Scaling laws and estimates are given in § 4.3. Alternative orderings of terms may apply for media with enhanced refraction from non-Kolmogorov structures.

The scaling of the pulse broadening time with frequency indeed shows departures for some objects from the scaling expected for a Kolmogorov medium (Löhmer et al. 2003). These departures either indicate actual departures from a Kolmogorov wavenumber spectrum or the breakdown of the assumption of an unbounded screen, which can give anomalous scalings (Cordes & Lazio 2001). Löhmer et al. (2004) conclude that anomalous scattering is associated with distant objects whereas nearby objects generally show Kolmogorov scalings (or nearly so). One such scaling is for the scintillation bandwidth $\Delta\nu_d$ with frequency (Cordes et al. 1985). Another is the slope of the structure function for DM (e.g. You et al. 2007).

4.4. *Frequency-dependent DM Variations From Multipath Screen Averaging*

Consider a simple screen model for the diffraction and refraction. The diameter of the scattering cone at a phase screen located a distance $D' = D - D_s$ from Earth for a pulsar distance D is $\ell_s \approx 2D'\theta_d$. Measurement of DM toward a source therefore involves spatial averaging over an area $\sim \ell_s^2$. This causes the measured DM to differ from that for the direct line of sight through the screen. Since $\theta_d \propto \nu^{-2.2}$ or so, this implies that the difference in DM is strongly frequency dependent. By defining a weighting function $W(\mathbf{x}, \nu)$ that is defined by the scattered image expressed with a spatial argument (i.e. $\mathbf{x} = D'\boldsymbol{\theta}$) and thus has a width $\sim \ell_s$, it can be shown that the rms difference in DM is a weighted integral over the phase structure function and

$$\delta\text{DM} \approx 10^{-1.05} \text{ pc cm}^{-3} \text{ SM } D'^{5/6}\nu^{-11/6} \tag{15}$$

for SM in standard units, D' in kpc, and ν in GHz. The resulting TOA perturbation, which is stochastic with characteristic time scale $\ell_s/V_{\text{eff}\perp}$ (the same time scale as for RISS), has rms

$$\Delta t_{\text{DM},\nu} \approx 0.12 \ \mu s \ D'^{5/6}\nu^{-23/6} \left(\frac{\text{SM}}{\text{kpc m}^{-20/3}} \right). \tag{16}$$

While small, this effect results from the dispersion measure effectively being a function of frequency. It is a steep, declining function of frequency because the area of the scattering cone decreases rapidly with frequency. The frequency dependence is nearly degenerate with some of the other timing errors.

4.5. *Pulse Broadening Function*

Pulse broadening from multipath scattering in the ISM is described by a pulse-broadening function (PBF) that is convolved with the emitted pulse shape to produce the measured pulse.

The ensemble average pulse-broadening function (PBF) has a characteristic width $\tau_d \sim D\theta_d^2/2c$ where θ_d is the diffraction angle and D is an effective distance. The timing perturbation is proportional to the width of the PBF, which is strongly wavelength dependent ($\propto \lambda^4$). The pulse broadening times in Figure 4 demonstrate that they are a strong function of both DM and frequency. The empirical fit from Bhat et al. (2004) is $\log \tau_d = -6.46 + 0.154 \log \text{DM} + 1.07 (\log \text{DM})^2 - (3.86 \pm 0.16) \log \nu$. The scatter about this fit is ± 0.65 in $\log \tau_d$.

We write the PBF as $p_d(t) = \overline{p}_d(t) + \delta p_d(t)$. where $\overline{p}_d$ is the ensemble-average shape[1] expected from a particular medium and consider it to be a slow function of epoch. By constrast, δp_d encapsulates fast departures from the ensemble average. Defining $p_d(t)$ to have unit area, the characteristic broadening time is

$$\overline{\tau}_d = \int dt\, t\, p_d(t) = \tau_d + \delta\tau_d, \tag{17}$$
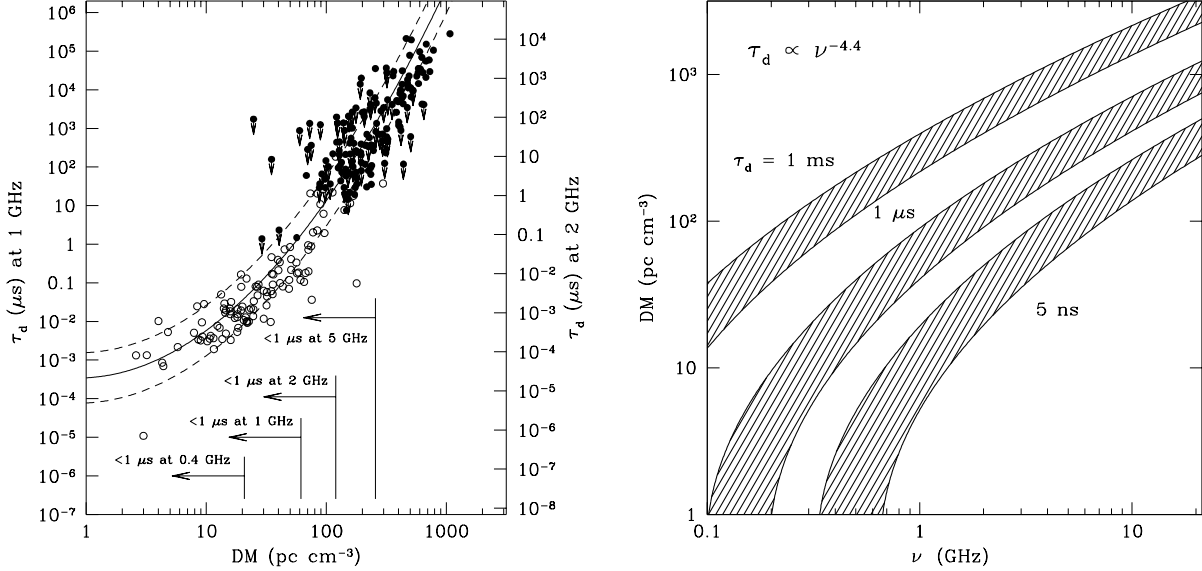
and its ensemble average as τ_d.

FIG. 4.— (Left) Pulse broadening time plotted against DM for pulsar data used to construct the NE2001 model (Cordes & Lazio 2002). The solid curve shows the parabolic fit given in the text for $\log \tau_d$. and the dashed curves show $\pm 1.0\sigma$ deviations from the fit. Open circles are inferred values using scintillation bandwidth measurements; filled circles are direct measurements of τ_d. Downward arrows denote upper limits. All measurements have been scaled to 1 GHz assuming $\tau_d \propto \nu^{-4.4}$ and the right-hand scale for 2 GHz assumes the same scaling. The strong scattering regime is assumed, which requires $\tau_d \gg C_1/2\pi\nu$ or $\tau_d \gg 2 \times 10^{-4}$ μs at 1 GHz. At lower frequencies, the entire range of τ_d in the plot satisfies the requirement. Leftward arrows designate maximum values of DM for which $\tau_d < 1$ ms at 0.4, 1 and 2 GHz using the nominal parabolic fit. (Right) Contours of constant pulse broadening time, τ_d, using the fit shown in Figure 4 including the $\pm 1\sigma$ uncertainty in the fit, which results in the widths of the shaded regions. A $\tau_d \propto \nu^{-4.4}$ scaling with frequency is used. This scaling is steeper than appropriate for some high DM objects but is typical for low-DM pulsars.

The scintillation bandwidth and the mean pulse broadening time $\overline{\tau}_d$ are related by[2]

$$2\pi\overline{\tau}_d\Delta\nu_d = C_1, \tag{18}$$

where C_1 depends on all the properties of the medium (Cordes & Rickett 1998; Lambert & Rickett 2000), such as the wavenumber spectrum, its thickness and location along the (LOS) and on its transverse extent (Cordes & Lazio 2001). For simple media, values of C_1 can be calculated. For a *thin screen* unbounded transverse to the LOS and with a circular Gaussian angular scattering function, the PBF is a one-sided exponential function with $1/e$ time scale τ_d. In this case the mean time delay is also τ_d so that $C_1 = 1$. For media that are plausibly relevant to pulsar scattering, C_1 can vary by a factor of nearly two (Cordes & Rickett 1998; Lambert & Rickett 1999).

4.6. *The Mean-Shift Regime*

[1]
  This might also be called a "snapshot" average using the language of Narayan & Goodman (1989), which takes into account that a statistically precise measurement at a given epoch is still not a good ensemble average because there are long-term refraction effects. Our approach is to treat refraction effects as a separate modulation imposed on a statistically precise average at a given epoch.

[2]
  Our definitions of $\Delta\nu_d$ and $\overline{\tau}_d$ follow Cordes & Rickett (1998), i.e. $\Delta\nu_d$ is the HWHM of the intensity ACF vs. frequency lag and $\overline{\tau}_d$ is the mean delay of the PBF. This differs from Lambert & Rickett (1999), who use alternative definitions of τ_d in a similar expression and thus quote different values of C_1 than we use here.

A case of interest for nearby pulsars or observations at high frequencies is where the pulse broadening time is small compared to the pulse width, $\tau_d \ll W$ but where the strong scintillation regime applies. This requires that the scintillation bandwidth $\Delta\nu_d \ll \nu$ or, equivalently, $\tau_d\nu \gg 1$. We specify the mean-shift regime as

$$\frac{C_1}{2\pi\nu} \ll \tau_d \ll W \qquad \text{or} \qquad 0.2 \text{ ns } \nu_{\text{GHz}}^{-1} \ll \tau_d \ll 1 \text{ ms } W_{\text{ms}}. \tag{19}$$

Under these conditions the TOA perturbation is simply the pulse broadening time calculated from Eq. 17 using the instantaneous PBF (not the ensemble-average PBF). The TOA perturbation also depends on the number of scintles contributing to an observation. In many cases it is large and the TOA perturbation converges to some mean value. This requires that $\Delta\nu_d \ll B$, where B is the bandwidth, or that $\Delta t_{\text{ISS}} \ll T$, where T is the total time of the observation. Figure 4 yields the range of DM for which the shift approximation applies: $\tau_d < 1$ ms for DM $\lesssim 100$, 250 and 400 pc cm^{-3} at 0.4, 1 and 2 GHz, respectively.

One approach to timing precision is to require that τ_d be smaller than some specified rms timing error, σ_{max}, which might be 100-ns or less for pulsar timing array applications but could be much larger for other timing purposes (such as pulsars in the Galactic center). If $\tau_d < \sigma_{\text{max}}$, pulse broadening might be ignored entirely. Alternatively, it might be corrected to a fractional precision ϵ_τ, yielding a residual error $\epsilon_\tau\tau_d < \sigma_{\text{max}}$. Using the empirical fit for τ_d vs. DM shown in Figure 4, we can then solve for DM(ν) for different σ_{max}. Results are shown in Figure 4. The smallest pulse broadening effects occur in the lower-right portion of the diagram whereas objects with large DMs are strongly affected by pulse broadening. Many pulsars have steep spectra, so the choice of frequencies for a given object requires a compromise, as discussed in § 6.

When the shift approximation holds, the TOA can be corrected by subtracting $\overline{\tau}_d$ from nominal values (Hemberger & Stinebring 2008). However, because by definition $\overline{\tau}_d$ is small, we cannot measure it directly at the frequency of the TOA measurements. There are several ways to estimate it, however.

4.6.1. Correlation Approach

The timing delay τ_d can be estimated by using Eq. 18, where the characteristic scintillation bandwidth $\Delta\nu_d$ is calculated as the half-width at half maximum of the intensity correlation function $\Gamma_{\delta I}(\delta\nu)$ that is calculated from the dynamic spectrum $I(\nu, t)$. This approach requires knowledge of the shape of the PBF so the type of medium must be known to determine the appropriate value for C_1. Alternatively, a characteristic time τ_{S_2} can be calculated from the secondary spectrum, the squared-magnitude of the Fourier transform of the dynamic spectrum (e.g. Stinebring et al. 2001), which is related to the autocorrelation function of the PBF. The relationship of τ_{S_2} to τ_d is also medium dependent and requires knowledge of their ratio that is analogous to knowing C_1. The correction of TOAs for the mean PBF delay is therefore problematic unless ancillary constraints on the scattering physics are known, namely whether a thin screen or extended-medium applies, whether the scattering region is bounded transverse to the LOS, what the wavenumber spectrum is, etc. The secondary spectrum provides much of this information (Stinebring et al. 2001; Hemberger & Stinebring 2008).

We identify the errors associated with this correction approach by considering Eq. 10 with an additional chromatic term, t_C, added. For the case where t_C consists solely of the pulse broadening term and the mean-shift regime applies, the TOA perturbation equals the pulse broadening time τ_d. The broadening time can be estimated from the scintillation bandwidth obtained at a frequency ν',

$$\widehat{\tau_d}(\nu') = \frac{\hat{C}_1}{2\pi\widehat{\Delta\nu_d}(\nu')}, \tag{20}$$

where quantities requiring an estimate or an assumed value are hatted. The broadening time can be scaled to other frequencies using

$$\widehat{\tau_d}(\nu) = \widehat{\tau_d}(\nu')\left(\frac{\nu}{\nu'}\right)^{-\hat{X}_{\text{PBF}}}. \tag{21}$$

The estimation error of the chromatic term and thus on t_∞ expands into terms dependent on individual errors, $\delta C_1, \delta\Delta\nu_d$, and δX_{PBF}:

$$\delta\tau_d = \tau_d - \widehat{\tau_d} \approx \tau_d\left[\frac{\delta C_1}{C_1} - \frac{\delta\Delta\nu_d}{\Delta\nu_d} - \delta X_{\text{PBF}}\ln\frac{\nu}{\nu'}\right]. \tag{22}$$

Based on estimates of scintillation bandwidths in the literature, the range of possible values of C_1, and the error in the exponent, δX_{PBF}, the combined error in $\delta\tau_d$ is unlikely to be less than 10% with this approach. However, a 10% error in removing pulse broadening implies that the shaded bands in Figure 4 will shift to the left by about a factor of 1.8 in frequency (0.26 in log ν).

4.6.2. *Phase Retrieval Methods*

A second, empirical approach requires much less *a priori* knowledge about the scattering medium. It calculates the complete PBF using only a measurement of the ACF of the PBF or, equivalently, the magnitude of the PBF's Fourier transform. The ACF of the PBF can be obtained from the secondary spectrum, for example. Walker et al. (2008) apply two-dimensional phase retrieval to the secondary spectrum and demonstrate the general principle. For the one-dimensional ACF with n_τ lags, there are n_τ functions that can produce the measured ACF. Many of these are acausal or include negative values and can therefore be ruled out. Those that remain include the function with minimum delay and its time reverse, which has maximum delay. Methods exist to calculate the *minimum-delay* PBF from the ACF, which is the unique member in the large family of PBFs consistent with the ACF that has its amplitude most concentrated toward the origin in a mean-square sense (Scargle 1981). While physically a minimum-delay solution is not demanded by scattering and refracting geometries, it may be the most probable result given that scattering and refraction angles have distributions peaked at zero. Also it may provide a more accurate correction compared to use of an idealized form for the PBF used to provide a value for C_1 in the correlation method. Application of inversion techniques will be explored in a separate paper (Cordes & Shannon, in preparation). Another approach (P. Demorest & M. Walker, private communication) investigates the phase of the wavefield directly to determine the PBF.

4.7. *Real World PBFs*

Time delays from pulse broadening presented so far represent ensemble-average results. TOAs, however, are determined from pulse profiles obtained as integrations over the time-frequency plane corresponding to the integration time T and bandwidth B. The $T-B$ plane contains a finite number of independent fluctuations ("scintles") of the diffractive interstellar scintillations (DISS), causing the instantanous PBF to differ from the ensemble average shape, producing a statistical error in the estimated TOA, as first demonstrated by (Cordes et al. 1990). In addition, because individual TOAs are typically estimated from data sets with no overlap in $T-B$, the TOA error is statistically independent and thus has a white-noise spectrum.

The TOA error arises from the summation of independent scintles in the $T-B$ plane, the number of which can be large or small when a pulse profile is obtained. In the following we will use $\Delta t_{\delta\text{PBF}}$ to mean both the specific value applicable to a particular TOA and also to signify its rms value, the context making it clear as which applies. The rms PBF error is approximately

$$\Delta t_{\delta\text{PBF}} = N_{\text{DISS}}^{-1/2}\tau_d, \tag{23}$$

where N_{DISS} is the effective number of "scintles." Previous work estimates N_{DISS} as

$$N_{\text{DISS}} = N_t N_\nu = (1 + \eta_t T/\Delta t_{\text{ISS}})(1 + \eta_\nu B/\Delta\nu_d), \tag{24}$$

where Δt_{ISS} is the characteristic DISS time scale and $\Delta\nu_d$ is the characteristic bandwidth, as before. The filling factors η_t, η_ν are less than unity and are in the range of 0.1 to 0.3, depending on the definitions of the characteristic time scale and bandwidth. In the following we use approximate values for η_t and η_ν while keeping in mind that the factorization of N_{DISS} is only an approximation. In another paper (Cordes & Shannon, in preparation), we derive exact results for several cases that validate the form of Eq. 23.

The scaling of the timing variation, $\Delta t_{\delta\text{PBF}}$, with frequency is different for the four cases where T and/or B are larger or smaller than the characteristic scintle size, i.e. whether N_t and/or N_ν are unity or much larger than unity and whether the scattering is strong or super-strong as defined in §4.3. In strong scattering $\tau_d \propto \nu^{-\zeta}$ where $\zeta = 2\beta/(\beta-2)$ for $\beta < 4$. From Eq. 18, the DISS bandwidth therefore scales as ν^ζ. For a Kolmogorov medium ($\beta = 11/3$), $\zeta = 22/5$. In super-strong scattering, the coherence length of the diffraction pattern is smaller than the inner scale and $\zeta \to 4$. Similarly, the characteristic DISS time scale scales as ν^κ with $\kappa = \beta/(\beta-2)$ in strong scattering and $\kappa = 2$ in super-strong scattering. The scaling depends on the type of medium (β), whether the scattering is strong or super-strong, and on the bandwidth and integration time relative to the DISS bandwidth and time scale. For a Kolmogorov medium the index x in $\Delta t_{\delta\text{PBF}} \propto \nu^{-x}$ ranges between 22/5 for low-DM pulsars observed at relatively high frequencies (but where the scattering is still strong) and 3/2 for high-DM pulsars observed at low frequencies in the super-strong scattering regime. This corresponds to the case where the scattered wavefield's coherence length is smaller than the inner scale of the wavenumber spectrum. In more detail we have the following cases: $N_t \ll 1$ and $N_\nu \ll 1$: $x = 22/5$; $N_t \gg 1$ and $N_\nu \ll 1$: $x = 19/5$; $N_t \ll 1$ and $N_\nu \gg 1$: $x = 11/5$; $N_t \gg 1$ and $N_\nu \gg 1$ and negligible inner scale: $x = 8/5$; $N_t \ll 1$ and $N_\nu \ll 1$ and where the diffraction scale is smaller than the inner scale: $x = 3/2$.

Figure 5 shows predicted values of $\Delta t_{\delta\text{PBF}}$ as a function of DM for Galactic coordinates, $\ell = 45°, b = 0°$, and particular observational parameters. The NE2001 model for the Galactic electron density (Cordes & Lazio

2002) was used to calculate Δt_{ISS} and $\Delta\nu_d$ vs. DM. Different curves correspond to different effective velocities that underly the scintillation time scale. The figure shows that the finite-scintle TOA perturbation increases rapidly for more distant pulsars and for observations at lower frequencies. The explanation is that even though the number of scintles increases rapidly, the pulse broadening time τ_d increases even faster.

4.8. *Large Pulse Broadening Times*

For distant pulsars observed at low frequencies and especially those with very narrow intrinsic pulses, the pulse broadening time can exceed the pulse width, causing strong distortion of th intrinsic pulse profile as well as delaying it. In this case, template fitting must be customized to each pulsar and frequency combination. Scintles are too narrow in time and frequency to resolve, so phase retrieval methods are not possible. One approach is to deconvolve the PBF from the measured pulse profile (e.g. Bhat et al. 2003) to yield the TOA along with determinations of the relevant PBF shape and the intrinsic pulse shape. This requires usage of a family of candidate PBFs for which the deconvolution indicates a best fit that is non-negative. The template bank of candidate PBFs needs to include those that are truncated since evidence exists, for highly scattered pulsars, that scattering screens are spatially truncated transverse to the LOS (Löhmer et al. 2004).

Consider a multifrequency timing program where the pulse broadening is larger than the pulse width W at lower frequencies and smaller than W at higher frequencies. The purpose of such a program may be to conduct precision timing by removing chromatic interstellar effects. The lower frequency measurements could be used to identify the form of the PBF, including its characteristic delay, and the frequency scaling of the delay. Corrections of the TOAs for the PBF delays and for a contemporaneous dispersion measure DM(t) calculated from the TOAs would then follow. This case is discussed explicitly in § 6.

Another case is where the pulse broadening is large at all frequencies in the program. This situation applies to pulsars in the Galactic center because radio scattering is particularly intense so that timing at radio frequencies $\lesssim 12$ GHz will not be in the mean-shift regime. TOA shifts from pulse broadening will depend in detail on the templates used. In addition, orbital motion that changes the distance to the scattering material that encloses the Galactic center will cause secular changes in the pulse broadening.
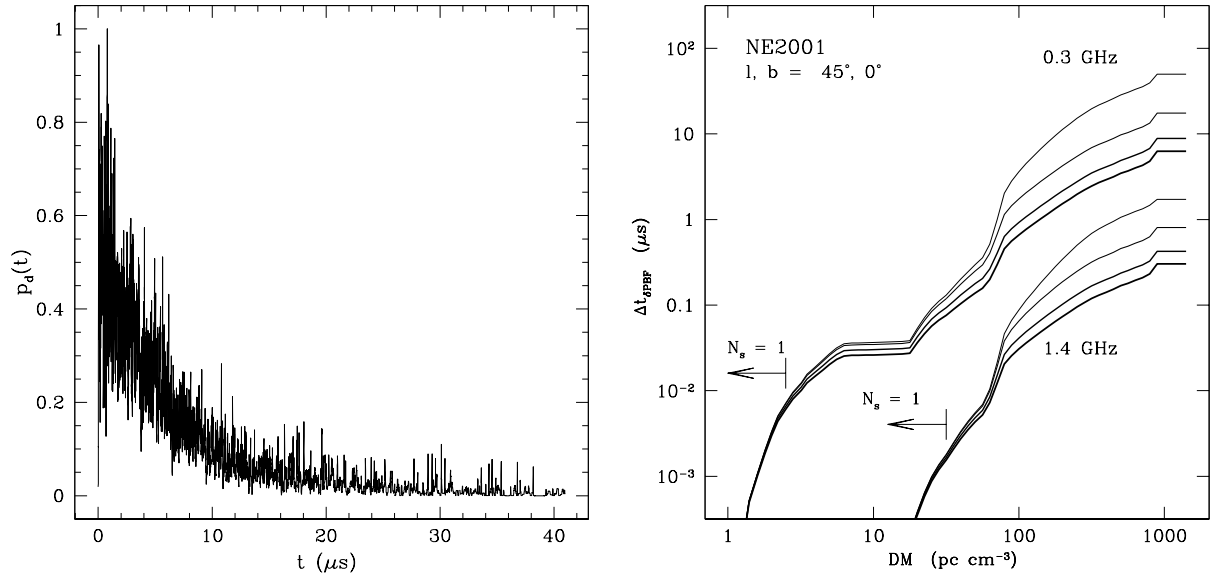

FIG. 5.— Left: Simulated pulse broadening function showing stochastic variations that result from the finite number of scintles in the time-frequency plane. This case is for a pulsar scattered into an rms angle of 1.25 mas by a screen 1 kpc from both the pulsar and the observer, an observation frequency and bandwidth of 1.4 and 0.1 GHz, respectively, and a total observing time of 2 hr. Details of the simulation are available on request. Right: Timing error due to variations in the pulse broadening function from the finite number of scintles. Results are shown for a LOS through the inner Galaxy ($\ell = 45°$, $b = 0°$) for two frequencies, 0.3 GHz and 1.4 GHz, with bandwidths of 50 MHz and 200 MHz, respectively. From top to bottom in each set, the curves are for effective velocities of 10, 100, 400 and 800 km s^{-1}. For lower velocities, there are fewer scintles averaged over the fixed observing time of $T = 300$ s so the timing error is larger. The arrows indicate values of DM for which the number of scintles sampled $N_s = 1$.

4.9. *Angle-of-Arrival and Refractive Scintillation Variations*

Structures in the ISM refract radiation if they are much larger than the Fresnel scale $\sqrt{\lambda D} \approx 10^{11}$ cm and larger than the so-called refractive or multipath scale $D_{\text{eff}}\theta_d \approx 1$ AU, causing the angle of arrival (AOA) to deviate from the direct path. Wavefront curvature caused by the same large-scale structures changes the flux density (Rickett 1990) to produce refractive interstellar scintillations (RISS). We give results here only for thin screen media, which serve as simple examples and allow scaling laws to be derived.

Let θ_r be the departure of the AOA from the direct path as viewed by an observer. The induced time delay for a fiducial refraction angle of 1 mas is

$$\Delta t_{\text{AOA}} \approx \frac{1}{2c}D_{\text{eff}}\theta_r^2 \approx 1.21 \ \mu s \ D_{\text{eff}}(\text{kpc})\theta_r^2(\text{mas}) \tag{25}$$

where D_{eff} is the effective distance through the ISM. For a thin screen at distance D_s from a pulsar at distance D from the Earth, $D_{\text{eff}} = (D - D_s)(D/D_s)$. (If the refraction angle is defined instead as the bending angle produced by the screen, the effective distance is $D_{\text{eff}} = (D - D_s)(D_s/D)$.) The delay scales as λ^4 if refraction is produced by a discrete cloud but scales slightly differently for a medium with a large range of scales (e.g. Cordes et al. 1986; Romani et al. 1986).

A second effect is associated with the transformation of the TOA to the SSBC (Foster & Cordes 1990), which depends on an assumed direction to the pulsar. Interstellar refraction causes the actual and true directions to differ, inducing a perturbation that scales as λ^2,

$$\Delta t_{\text{AOA,SSBC}} = c^{-1}\hat{n} \cdot \mathbf{r}_\oplus \approx c^{-1}r_\oplus\theta_r(t)\cos\Phi(t) \approx 2.4 \ \mu s \ \theta_r(\text{mas})\cos\Phi(\text{t}), \tag{26}$$

where $R_\oplus/c \approx 500$ s and $\Phi(t)$ is the cyclical angle between the LOS $\hat{n}$ and the Earth-SSBC vector.

The last effect results from distortion of the scattered image of the source caused by wavefront curvature, which modulates the integrated flux by a factor $G = G_x G_y$, where $G_{x,y}$ are "gain" variations related to the second phase derivatives of the refractive phase in the x, y directions. For simplicity, we assume that the scattered image would be circularly symmetric in the absence of wavefront curvature ($G_{x,y} = 1$), yielding a mean delay $\overline{\tau}_d^{(\text{iso})}$. For $G_{x,y} \neq 1$ the mean delay becomes

$$t_{\text{PBF,RISS}} = \frac{1}{2}\overline{\tau}_d^{(\text{iso})}(G_x + G_y), \tag{27}$$

as shown in Appendix B. Since refractive flux variations are typically tens of percent but can extend to 100% or more, this timing modulation can be a large fraction of the mean PBF delay. The variations induced by the gains scale as $G_{x,y}^{-1} - 1 \propto \lambda^2$. Combined with the $\lambda^{4.4}$ scaling of $\overline{\tau}_d$, the refraction-induced variations in τ_d are very strongly frequency dependent. Variable pulse broadening on a time scale of ~ 60 to 200 days was reported for the MSP B1937+21 at the 20% level (Cordes et al. 1990; Ramachandran et al. 2006) that has been attributed to refractive modulation of diffraction, as described here.

5. A SIGNAL MODEL FOR PULSE ARRIVAL TIMES

We combine the physical TOA errors highlighted in §§ 3-4 into groups that are convenient for discussing the overall timing error budget and for fitting to multi-frequency arrival times. The total TOA perturbation has two terms,

$$\Delta t_{\text{TOA}} = \Delta t_{\text{W}} + \Delta t_{\text{slow}}, \tag{28}$$

one with white-noise statistics and a second that varies slowly enough that it is typically correlated between observing epochs. A careful analysis of the errors must also consider the frequency dependences of the various terms. The white-noise term is

$$\Delta t_{\text{W}} = \Delta t_{\text{J}} + \Delta t_{\delta\text{PBF}} + \Delta t_{\text{S/N}}. \tag{29}$$

The slow term is made up of strongly chromatic contributions,

$$\Delta t_{\text{slow}} = \Delta t_{\text{DM}} + \Delta t_{\text{PBF}} + \Delta t_{\delta\text{PBF,RISS}} + \Delta t_{\text{AOA}} + \Delta t_{\text{AOA,SSBC}} + \Delta t_{\text{DM},\nu} + \Delta t_{\text{RM}}. \tag{30}$$

The two terms (white and slow) are treated very differently in any arrival time analysis. The white-noise terms are unavoidable because they cannot be fitted for and subtracted from arrival times. The slow terms, unlike the white terms, can potentially be removed through appropriate multi-frequency fitting because there is a finite number of contributing terms that have different frequency scalings. Timing noise and gravitational perturbations also produce slow variations but are achromatic.

We now discuss the white-noise and slowly varying terms in detail.

5.1. *White Noise Contributions to Timing Errors*

Pulse-phase jitter, the finite-scintle effect and radiometer noise are typically uncorrelated between data sets used to estimate individual TOAs. Jitter is weakly chromatic, while the other two contributions are strongly chromatic. For radiometer noise, this is due partly to the contribution of Galactic synchrotron noise at frequencies less than about 0.5 GHz and to the typical steepness of pulsars' radio spectra. However, when interstellar scattering broadens the pulse at low frequencies, the radiometer-noise error is enhanced according to Eq. 3 because the pulse-width increases and SNR_1 decreases. Scintillations are strongly chromatic.

In Figure 6 we show the three white-noise terms for four different sets of pulse period and DM. The salient features of the cases shown in the figure are that

1. For fixed observing time T, the phase-jitter effect is small for MSPs that have narrow pulse widths and for which a TOA is calculated from a large number of pulses. The opposite is true for strong, long-period pulsars, which will have jitter dominated TOA errors at frequencies $\gtrsim 0.4$ GHz.

2. The radiometer noise term $\Delta t_{S/N}$ dominates other TOA perturbations for weak pulsars (or observations with small telescopes). At low frequencies, the timing error is enhanced by pulse broadening from ISS, which also reduces the peak flux density.

3. For strong pulsars, the TOA error is dominated by radiometer noise at low frequencies because of the large Galactic background and by pulse jitter (Δt_J) at high frequencies. In some cases (e.g. the bottom-left panel in Figure 6) at intermediate frequencies $\sim 0.5 - 2$ GHz, the finite scintle effect (Δt_{PBF}) plays a role.

4. At higher frequencies, the TOA errors of weak, short period pulsars are dominated by radiometer noise unless high-gain telescopes (Arecibo, SKA Phase 1, SKA) are used.

The primary recourse is to reduce the amplitudes of the three contributing terms by increasing the averaging time and the bandwidth and by improving the sensitivity of the telescope with a larger collecting area or reduced system noise temperature. As a function of frequency $\Delta t_{S/N}$ and $\Delta t_{\delta PBF}$ are typically uncorrelated (in the latter case for bandpasses that are separated by at least one scintillation bandwidth). The jitter term Δt_J is correlated even between widely spaced frequencies because single pulse structure is typically seen over octave bandwidths, though not without some evolution in frequency. A multifrequency analysis may be useful for correcting or reducing pulse phase jitter owing to this partial correlation.

5.2. *Slow, Chromatic Variations*

The slow terms in Eq. 30 are all caused by plasma effects and are therefore strongly chromatic. From left to right, the terms scale with frequency approximately as $\nu^{-2}, \nu^{-4.4}, \nu^{-X}, \nu^{-4}, \nu^{-2}, \nu^{-23/6}$ and ν^{-3}. We emphasize that such scalings are idealized and likely differ between lines of sight and also for particular realizations of sampled data.

In the absence of multipath scattering, the DM term scales as ν^{-2} with departures that require very high electron densities or frequencies near the plasma frequency $\propto \nu^{-4}$ (Tanenbaum et al. 1968; Craft 1970). However, multipath scattering introduces an averaging scale on the DM perturbation that adds the small term with $\nu^{-23/6}$ frequency dependence, as discussed in § 4.4.

The $\nu^{-4.4}$ scaling of Δt_{PBF} assumes a Kolmogorov wavenumber spectrum in the moderate scattering regime. In super-strong scattering the exponent becomes -4 because the diffraction scale is much less than the inner scale. This regime will apply for high-DM pulsars observed at low frequencies. Other departures from the $\nu^{-4.4}$ scaling for pulse broadening mentioned earlier (Löhmer et al. 2001, 2004) indicate that the ISM has more complex structure than in idealized models.

The scaling of the AOA term $\propto \nu^{-2}$ also requires discussion. For discrete structures in the ISM that refract the diffracted radiation from a pulsar, this scaling is appropriate. However, the scaling differs for density irregularities from a Kolmogorov spectrum because the range of length scales contributing to the refraction also varies with frequency. For a Kolmogorov spectrum, refraction effects are small, however, so it is appropriate to model the AOA term as we have, given that there is evidence for the presence of non-Kolmogorov refracting structures in the ISM (Hill et al. 2005).

The frequency scaling of the RISS modulation of pulse broadening is not a simple power law because the dependence on the gains $G_{x,y}$ and on any anisotropy in the diffraction is not simple. However, in

the following we assume an approximate scaling law, $\nu^{-X_{\delta\mathrm{PBF}}}$ for this term that applies over a restricted frequency range.

The RM term is likely too small to include in any actual fitting model for most lines of sight. It is conceivable that a pulsar of interest will be discovered for which profile splitting is important because the RM is large. The actual scaling law of the timing perturbation may differ from the generic ν^{-3} scaling because any effect will depend on how TOAs are calculated from the measured pulse profiles in the various Stokes parameters.

We write terms using values at a fiducial frequency, ν_0. In approximate order of decreasing amplitude we have, using $z \equiv \nu/\nu_0$,

$$\Delta t_{\mathrm{slow}}(t,\nu) = \Delta t_{\mathrm{DM0}}z^{-2} + \Delta t_{\mathrm{AOA,SSBC}_0}z^{-X_{\mathrm{AOA}}} + \Delta t_{\mathrm{PBF0}}z^{-X_{\mathrm{PBF}}} + \Delta t_{\mathrm{AOA0}}z^{-2X_{\mathrm{AOA}}}$$

$$+ \Delta t_{\delta\mathrm{PBF,RISS}_0}z^{-X_{\delta\mathrm{PBF}}} + \Delta t_{\mathrm{DM},\nu_0}z^{-X_{\mathrm{DM},\nu}} + \Delta t_{\mathrm{RM0}}z^{-3}, \tag{31}$$

where, for example, for a Kolmogorov medium in strong scattering, $X_{\mathrm{PBF}} = 4.4$, $X_{\mathrm{AOA}} = 2$, $X_{\mathrm{DM},\nu} = 3.8$ and $X_{\delta\mathrm{PBF}}$ has a number of possible values as described earlier.

6. MITIGATION OF TIMING ERRORS FROM NON-DISPERSIVE CHROMATIC EFFECTS

We have identified salient timing errors that are introduced by intervening plasmas. The primary question is how to contend with them when precision timing is required, as for the detection of gravitational waves with pulsars. We discuss two broad approaches that are based on fitting "raw" arrival times vs. frequency ν (as opposed to first correcting TOAs for one or more effects with subsequent fitting).

An augmented version of Eq. 10 for the TOA includes a non-dispersive, chromatic term, t_C,

$$t_\nu = t_\infty + t_{\mathrm{DM}}(\nu) + t_C(\nu) + t_{\mathrm{W}}(\nu). \tag{32}$$

To simplify the notation, we have dropped the 'Δ' used previously to represent fluctuations. In the following we consider multifrequency TOAs at a given epoch. Consequently we include in t_{W} only the radiometer noise and scintillation effect. The jitter term in this context is considered to be frequency independent (see § 3.3). When using the variance of the white noise in weighted least-squares fitting across frequency, we exclude the jitter term for this reason. However, the jitter term does contribute to epoch-to-epoch timing errors, as previously discussed.

6.1. Ignore Refraction and Scattering Effects

One approach is to simply ignore all effects other than the dispersion delay. Most arrival-time analyses to date include the dispersive term Δt_{DM} as the only chromatic perturbation. Such programs use dual or multiple-frequency TOAs to estimate DM at each epoch or use ancillary measurements of DM to correct TOAs to infinite frequency at the SSBC. This procedure allows scattering to contaminate the estimated TOA (Foster & Cordes 1990). To be successful, removal of dispersion delays only requires additional errors to be smaller than some target precision. As in Figure 4 for the case of pulse broadening, restrictions can then be made on the combination of observation frequencies and DMs of a pulsar sample that can satisfy the error budget.

Following the same approach discussed in § 4.1 and in Appendix D, we calculate the error on the corrected TOA, t_∞, when the t_C term is present in the data but only the t_{DM} term is included in the fit. For example we consider the simple case where that t_C includes only one term instead of the many terms of Eq. 31 and that it scales as $t_C(\nu) = a_C \nu^{-X}$, (where we drop any subscript on the exponent, X). The two parameter fit for t_∞ and DM yields a systematic error for t_∞ (in addition to the random, standard error) that can be written as

$$\delta t_\infty = -a_C R_{t_\infty}, \tag{33}$$

where R_{t_∞} is a coefficient defined in Eq. D3. For $X = 4$, a 2:1 range of frequencies, and frequency channels ranging in number from 2 to 1024, we find a variation $R_{t_\infty} \approx 0.3 \pm 0.05$. Thus a fraction $1 - R_{t_\infty} \sim 70\%$ of the non-dispersive delay a_C is absorbed in the fit for DM, yielding an estimate for t_∞ that is too early by $\sim (0.3 \pm 0.05)a_C$. For a 4:1 frequency range, $R_{t_\infty} \approx -0.1$, so 90% of a_C is absorbed. However, for a 1.5:1 range, only about 50% is absorbed in the fit. Referring to Figure 4 for a 2:1 frequency range, the maximum timing error σ_t from this effect alone requires that $a_C < \sigma_t/R_{t_\infty}$ or, since $a_C \equiv t_C(\nu_1)\nu_1^X$,

$$t_C(\nu_1) < \nu_1^{-X} R_{t_\infty}^{-1} \sigma_t. \tag{34}$$

For $\nu_1 = 2$ GHz, $\sigma_t = 0.1$ μs and using $R_{t_\infty} = 0.3$, we need $t_C(2 \text{ GHz}) < 19$ ns.

A more detailed analysis is shown in Figure 7 with calculated results for an MSP with $P = 1.5$ ms with low DM (10 pc cm^{-3}) with Galactic coordinates $\ell, b = 45°, 0°$ and a pulse width of 50 μs. The period-averaged

flux density is 1 mJy at 1.4 GHz and scales with frequency as ν^{-2}. The NE2001 model is used to estimate the distance and pulse broadening from scattering. In the left hand panel, the rms timing error is plotted against bandwidth B for the case of an MSP observed with a 100-m class telescope. The right-hand panel shows the corresponding errors for DM. The example shown in the figure applies to observations using 100-m class telescopes. The highest frequency in the example is 2 GHz so the measurements and fit therefore cover the frequency range $[2 - B, 2]$ GHz for each bandwidth plotted. The left-hand panel shows standard errors for fitting functions with one to three parameters (t_∞, DM and a_C) and systematic errors for the three cases. Other details are described in the caption. The two-parameter fit is relevant to this section where pulse broadening is ignored. Salient features of the figure include:

1. For the $k = 2$ fit for t_∞ and DM the total error minimizes at $B \approx 1.4$ GHz as pulse broadening becomes important at the lower frequencies in the band.

2. When pulse broadening is ignored in any fitting, the best approach is to use a two-parameter fit if DM is not known to suffcient precision to warrant a single-parameter fit.

3. For small bandwidths, standard errors (dashed lines labeled $\sigma_{\mathrm{SE,k}}$, $k = 1, 2, 3$) become increasingly larger in going from one to three-parameter fits because the weak dispersive and scattering terms are not well modeled. The timing error scales as $B^{-1/2}, B^{-3/2}$ and $B^{-5/2}$, respectively, when the TOA error is dominated by radiometer noise, as it is for small bandwidths. For $B \ll \nu_1$ the ratio $\sigma_{\mathrm{SE,2}}/\sigma_{\mathrm{SE,1}} \approx \sqrt{3}\nu_1/B$ and is a factor of 69 for the smallest B plotted in Figure 7. The penalties for fitting for DM and t_C can be avoided if the dispersion measure and pulse broadening are known to sufficient accuracy from ancillary measurements, but both of these quantities vary with epoch and must be monitored.

4. Foreshadowing results in the next section, the three parameter fit improves the TOA error but only if the scaling exponent X is known. The upturn in $\sigma_{T,3}$ is caused by a 10% uncertainty in X, $\delta X = 0.44$, illustrating the requirements on prior knowledge of X. Nonetheless the improvement is by a factor of about 10 and can be greater if X is known to better precision.

5. The best achievable timing precision corresponds to $\sigma_{T,3}$ and is about 0.1 μs for the 600-s observation shown and with a 1.8 GHz bandwidth.

6. Brighter pulsars will shift the curves downward over most, but not all of their plotted range.

We emphasize that the results shown in Figure 7 and in the next two figures do not include all refraction and diffraction effects, so they must be taken as illustrative and optimistic for considerations of ISM effects alone.

6.2. *Aggressive Removal of Refraction and Scattering Effects*

If non-dispersive effects are tackled more aggressively, a larger number of pulsars can be included in a timing program because a wider range of frequency-DM combinations can satisfy a given error budget.

Consider the case where, along with t_∞ and t_{DM}, we include t_C in the fitting function as a power-law $t_C = a_C \nu^{-X}$.

This approach does not require knowledge of C_1 or measurement of the scintillation bandwidth $\Delta\nu_d$ as discussed in § 4.6.1 but it does require assumption of a value for the exponent, X. For now, we consider X to be known and we consider t_C to describe only pulse broadening.

Figure 8 shows results similar to those in Figure 7 for observations with $\nu_1 = 2$ GHz of a 1.5 ms pulsar at DM $= 100$ pc cm^{-3} using a 100-m class telescope (left panel) and a 300-m class telescope. The latter case corresponds approximately to the Arecibo telescope, the Chinese FAST telescope, and the proposed Phase 1 of the SKA.

The standard errors shown in the figure are larger for the 100-m class telescope in accord with its smaller sensitivity by about a factor of four. The total error from the two-parameter fit minimizes for $B \approx 0.5$ GHz and $B \approx 0.4$ GHz for the smaller and larger telescopes, respectively, the upturn being caused if there is no correction for pulse broadening. A similar upturn occurs for the three parameter fit if there is an error in the scaling-law exponent $\delta X = 0.44$ (10%). If there is no error, the best rms error is for a bandwidth $B = 1.6$ GHz and is approximately 2.5 times better for the larger telescope.

The conclusions that can be made from this particular case are that aggressive treatment of pulse broadening can drastically improve timing precision of moderate-DM pulsars and thus allow more pulsars to be included

in a pulsar timing array than otherwise would be the case. Without addressing pulse broadening, there is a maximum usable bandwidth that is less than 1 GHz and the timing precision $\sim 1~\mu s$ is not competitive for PTAs unless more observations are made during a year.

Figure 9 compares observations of a high DM pulsar (500 pc cm^{-3}) at high frequency (5 GHz) for observations with an Arecibo-class instrument (left panel) and an SKA-class instrument (right panel). For the SKA we have used a nominal sensitivity $A_{\mathrm{eff}}/T_{\mathrm{sys}} = 10^4$ m^2 K^{-1}. Note that the spin period in this case is 3 ms. The results indicate that aggressive fitting for pulse broadening can yield timing precision that is competitive for PTA applications even for a high-DM object.

The examples shown in Figures 7 - 9 that include only pulse broadening can be used as a guide for how to deal with the other chromatic terms in Eq. 31. In total there are eight unknowns to be solved for at each epoch when we include the achromatic term t_∞. However, the RM term can almost always be ignored. The term $\Delta t_{\mathrm{AOA,SSBC}}$ is or almost is degenerate with the DM term in its frequency dependence $\propto \nu^{-2}$ and three of the other chromatic terms ($\Delta t_{\mathrm{PBF}}, \Delta t_{\mathrm{AOA}}$ and $\Delta t_{\mathrm{DM},\nu}$) are degenerate with scalings close to ν^{-4}. This suggests a minimum of four unknowns that require four measurements at each epoch over a frequency range that is adequate to solve for the unknowns. Additional terms can be fitted for to potentially improve the net timing precision. However, examples shown in the figures indicate that the "cost" of extra parameters is high and that the amplitudes of additional effects need to be large enough to surpass the cost in precision.

6.3. *Comparison with Well-timed MSPs*

We compare our predictions with actual measurements on four prominent MSPs to further illustrate timing budget considerations. All four objects show TOA precision of 200 to 300 ns in 5 min averages (Hotan et al. 2006) where, to be explicit, we mean the precision of the TOA estimate and not necessarily the rms residual over a time span of years. Three objects (J0437−4715, J1713+0747, and J1909−3744) show rms timing residuals that, when integrated over ~ 1 hr, are below 100 ns. The fourth, B1937+21 (J1939+2134), is bright but shows timing noise consistent with that seen in canonical pulsars, which is caused by torque variations. We use flux densities, pulse widths and other parameters from Hotan et al. (2006) and other references, as noted, and use parameters for the Parkes telescope and the 48 MHz bandwidth and 300-s integration time used by Hotan et al. (2006).

J0437−4715 is the brightest of the four pulsars, with a period-averaged flux density $S_{1400} = 137$ Jy. Eq. 3 combined with the pulse width $W = 85~\mu s$ and the system noise of the Parkes telescope ($S_{\mathrm{sys}} = 29$ Jy) predicts $\Delta t_{\mathrm{S/N}} = 13$ ns and $\Delta t_{\mathrm{J}} = 105$ ns. This object, not surprisingly, is very heavily jitter dominated. The low-DM (2.6 pc cm^{-3}) implies that interstellar effects will be much smaller than either of these leading effects. Increases in sensitivity with larger bandwidths or larger telescopes will not improve the TOA precision, but longer integration times and a larger numbe of TOAs will.

J1713+0747 is less bright and has a larger DM (16 pc cm^{-3}) than J0437−4715. For the Parkes telescope, the radiometer noise TOA error is about 50% larger than the jitter error (100 ns vs. 65 ns), but for larger telescopes jitter will dominate. Diffractive interstellar scintillations will strongly modulate the signal level at most frequencies, making even the Parkes measurements jitter dominated some of the time.

J1909−3744 is one of the best timing pulsars. The low DM (10.4 pc cm^{-3}) is similar to that shown in Figure 7 and implies that interstellar effects are small at frequencies above 1 GHz. The measured rms residual is $\sigma_t = 0.3~\mu s$. We estimate $\Delta t_{\mathrm{S/N}} \approx 0.41~\mu s$, consistent with the curve labeled 'S/N' in Figure 7 (left-hand panel) for the bandwidth used and after taking into account the small differences in values for period, width, flux density and system noise as well as the radio frequency and spectral index. Bailes (2007) notes that the pulsar flux density varies from DISS by a factor of 30 and Jacoby et al. (2005) exclude TOAs with errors in excess of 1 μs. The difference between the predicted and actual rms residual is attributable to modulations by DISS and by RISS. The narrow pulse for this object (42 μs) implies that pulse jitter does not make a significant contribution to the observed measurements ($\Delta t_{\mathrm{J}} \approx 27~ns$ from Eq. 5) unless the scintillated flux becomes very large.

The fourth object, B1937+21, has the shortest period (~ 1.6 ms) and narrowest pulse (30 μs) of the four objects we consider. It also has the largest DM (71 pc cm^{-3}) and is fairly bright. For the Parkes telescope, the TOAs are noise dominated with estimates $\Delta t_{\mathrm{S/N}} = 56$ ns and $\Delta t_{\mathrm{J}} = 19$ ns but will be jitter dominated for most larger telescopes. As noted earlier (§ 3.2), jitter in this object is ambiguous, displayed in giant pulses but not in typical pulses, so our estimate of Δt_{J} is uncertain and there is the possibility, not yet demonstrated, that timing precision can be improved by excluding giant pulses from timing estimates or by otherwise correcting for them.

7. SUMMARY AND CONCLUSIONS

Table 2 summarizes how timing precision may be limited by different causes and what the course of mitigation might be. We include timing noise intrinsic to the pulsar because many pulsars will in fact have timing residuals that are dominated by timing noise unless it can somehow be removed (e.g. Lyne et al. 2010).

For many objects, timing precision will be limited by a combination of radiometer noise and pulse-to-pulse phase jitter intrinsic to the pulsar. We have summarized the levels of jitter in different pulsars as presented in the literature and we have presented specific results on the bright MSP, J1713+0747. We have also shown the relationship between jitter and pulse-shape stability. The theoretical best timing precision is achieved when it is limited by additive white noise alone and it is straightforward to calculate the rms timing error $\Delta t_{S/N}$ using a pulsar's template pulse shape (Appendix A). Comparison of actual TOA errors against $\Delta t_{S/N}$ shows that for all pulsars except the MSP B1937+21 (Jenet & Gil 2004), the rms phase jitter appears to be a significant fraction of the pulse width and thus will limit timing when the signal-to-noise ratio is high.

In the *noise dominated regime*, TOA precision may be improved by actions that favorably alter any factor in Eq. A1: increasing the sensitivity (i.e. reducing S_{sys}) and the total bandwidth to increase the signal-to-noise ratio; improving dispersion removal to minimize the effective pulse width W; and increasing the number of pulses summed. In the *jitter dominated regime*, however, TOA precision is improved only by summing more pulses. Thus in either regime, an increase in telescope time per object is needed to decrease the timing errors from radiometer noise or jitter. As more sensitive instruments are built, more pulsars will have jitter-dominated timing, as we have shown in § 3.3. With the Square Kilometer Array, for example, most of the known canonical pulsars and the majority of MSPs will have jitter-dominated TOAs. Consequently, the SKA can be used with sub-arrays in order to increase the amount of observing time per object with the sensitivity of a sub-array set so that the TOAs are jitter dominated by only a small factor.

Timing variations from interstellar dispersion and scattering need to be characterized for each LOS owing to the richness of structure in the ISM. Low-DM pulsars (e.g. $\lesssim 50$ pc cm^{-3}) are clearly better for precision timing at frequencies ~ 1 GHz but the maximum DM is smaller for lower frequencies. For pulsar-timing array applications that use an ensemble of MSPs, the best approach is to find spin-stable MSPs with small dispersion measures. However, intrinsic spin noise in MSPs (Shannon & Cordes 2010) may require usage of higher-DM MSPs and mitigation of interstellar effects. We have shown that multiple frequency fitting of TOAs obtained over a large total range of frequencies can extend the allowed sample of pulsars. Objects in relativistic binaries are rare enough that future discoveries are likely to include pulsars with large DMs. The most extreme case is for pulsars orbiting the Milky Way's central black hole, Sgr A*, which will show extreme levels of scattering with corresponding large timing variations (e.g. Deneva et al. 2009).

The dominant interstellar timing error is from variations in DM followed by diffractive pulse broadening and its variations. Both of these effects are correctable to vary degree. Additional interstellar terms imply that timing measurements at a minimum of four narrowband frequencies over approximately a 2:1 frequency range. Better yet — and now feasible — are continuous measurements over octave-like frequency ranges. For small dispersion measures. the pulse broadening time is too small to be determined from TOAs alone even though it is large enough to influence the arrival times. We have outlined a procedure that fits nominal TOAs at multiple frequencies to remove chromatic effects. However, other approaches, also mentioned here, could alternatively remove some of the chromatic effects at individual frequencies before doing any multiple frequency fits. Further exploration is needed on using dynamic spectra and their analysis using either correlation functions or a secondary spectrum analysis (e.g. Hemberger & Stinebring 2008) to provide the

TABLE 2
REGIMES FOR PULSAR TIMING LIMITATIONS

Limiting Effect	Spectral Signature in TOAs	Regime Specifications	Mitigation
Timing noise	red	spin, torque noise	more pulsars in timing array, remove torque variations
Low S/N	white	weak pulsar, small telescope	larger T, B; smaller S_{sys}
Phase jitter	white	large S/N	larger T
Diffractive scintillations (Finite scintle effects)	white	moderate DM	large T, B, ν
S/N + pulse broadening	white	large scattering	larger ν or reject pulsar
DM, AOA variations	red	moderate DM objects	multi-frequency fitting
PBF + variations	red	slow changes in τ_d	multi-frequency fitting

necessary timing corrections. Other approaches that use phase information in high resolution sampling (e.g. P. Demorest, W. van Straten & M. Walker, private communication) also need to be explored.

APPENDIX

A. TIME-OF-ARRIVAL ERRORS FROM PULSE PROFILE STOCHASTICITY

Here we give expressions for the error in time of arrival (TOA) due to additive radiometer noise and to pulse-phase jitter that is intrinsic to the pulsar.

Radiometer noise is additive in the limit of large time-bandwidth product and causes a minimum error when matched filtering is used to estimate the TOA. Let $U(t)$ be the pulse waveform as a function of time and normalized to unity amplitude. Also define the autocovariance function of the noise to be $\rho(\tau) \equiv \langle n(t)n(t+\tau)\rangle/\sigma_{noise}^2$ such that $\rho(0) = 1$ and its characteristic width is $\Delta \equiv \int d\tau\,\rho(\tau)$. For a signal-to-noise ratio SNR (pulse maximum/rms noise), the rms timing error is (Downs & Reichley 1983)

$$\Delta t_{\rm S/N} = \frac{\left[\int \int dt\,dt'\,\rho(t-t')U'(t)U'(t')\right]^{1/2}}{{\rm SNR}\int dt\,[U'(t)]^2} = \frac{W_{\rm eff}}{{\rm SNR}_1\sqrt{\rm N}}\left(\frac{\Delta}{W_{\rm eff}}\right)^{1/2} = \frac{S_{\rm sys}}{S_{\rm peak}\sqrt{2B}}\left(\frac{W_{\rm eff}}{N}\right)^{1/2}. \quad (A1)$$

where $U' \equiv dU/dt$. The second equality holds in the limit where noise decorrelates on a time scale Δ much less than the pulse width, i.e. $\Delta \ll W$ for which $\rho(t) = \Delta\delta(t)$ and where the effective pulse width is $W_{\rm eff} = 1/\int dt[U'(t)]^2$; the result is written in terms of the SNR for a single pulse and the number of pulses summed, ${\rm SNR}_1 = {\rm SNR}/\sqrt{\rm N}$. The third form shows that the error does not depend on Δ, where we have used $S_{\rm sys}$ as the system equivalent flux density, $S_{\rm peak}$ as the average peak flux density of a pulse, and B is the total bandwidth. The factor of two accounts for summing of two polarization channels.

For measured pulse profiles $U_j = U(j\Delta t)$ sampled discretely at intervals $\Delta t \ll W_{\rm eff}$, the effective width can be calculated by differencing,

$$W_{\rm eff} = \frac{\Delta t}{\sum_j (U_{j+1} - U_j)^2}. \quad (A2)$$

The denominator is proportional to the structure function of the pulse profile. If the sampled pulse has finite signal-to-noise ratio, the denominator must be corrected for the additive noise by subtracting $2n_{\rm on}\sigma_n^2$, where σ_n is the rms of the additive noise and $n_{\rm on}$ is the number of terms in the sum. For a Gaussian pulse with width W (FWHM),

$$\Delta t_{\rm S/N} = \frac{W}{(2\pi\ln 2)^{1/4}{\rm SNR}_1\sqrt{\rm N}}\left(\frac{\Delta}{W}\right)^{1/2}. \quad (A3)$$

We describe jitter by letting $a(\phi)$ be the functional form of a single pulse and $f_\phi(\phi)$ the probability density function (PDF) for the phase pulse-to-pulse phase jitter. Assuming all pulses have the same shape, the ensemble-average pulse shape is

$$U(\phi) \propto \int d\phi'\,f_\phi(\phi')a(\phi - \phi'). \quad (A4)$$

With this model and the phenomenologically consistent assumption that an infinite pulse average converges to $U(\phi)$, the TOA error is (using the pulse period P)

$$\Delta t_{\rm J} = N_i^{-1/2}(1 + m_I^2)^{1/2}\,P\langle\phi^2\rangle^{1/2} = N_i^{-1/2}(1 + m_I^2)^{1/2}\,P\left[\int d\phi\,\phi^2 f_\phi(\phi)\right]^{1/2}, \quad (A5)$$

where $N_i \le N$ is the number of *statistically independent* pulses that have been summed and m_I is the intensity modulation index (ratio of rms intensity to mean intensity), typically of order unity. Intensity fluctuations without phase jitter yield no timing error but they enhance timing errors when there is phase jitter. Letting $\langle\phi^2\rangle^{1/2} \equiv \xi_U f_J W_i/P$ we define a dimensionless jitter parameter f_J equal to the width (FWHM) of the phase-jitter PDF in units of the resulting *intrinsic* pulse width W_i, where $\xi_U \sim 1$ is a shape-dependent factor. For Gaussian shaped pulses with a Gaussian phase jitter distribution, we obtain

$$\Delta t_{\rm J} = \frac{f_J W_i(1 + m_I^2)^{1/2}}{2(2N_i\ln 2)^{1/2}}. \quad (A6)$$

This idealized result will also apply approximately to pulsars with multicomponent profiles. The amplitudes and phases of individual subpulses in different components are only partially correlated, so a profile with M components would show a jitter-induced error that is up to a factor $M^{-1/2}$ smaller than that for a single component.

B. SCATTERING AND REFRACTION FROM THIN SCREENS

Electron-density fluctuations on large scales refract, focus and defocus radiation from a pulsar producing variations in flux density and arrival time. "Large" is defined relative to the scale $\sim D\theta_d$ that is larger than the Fresnel scale $\sim \sqrt{\lambda D}$ by the same factor that the Fresnel scale is larger than the diffraction scale $\sim \lambda\theta_d$. (e.g. Rickett 1990). While an acceptable model for electron-density variations is one with a continuum of length scales, it is useful to separate large and small scales, as we do here. The Kirchoff diffraction integral for the scalar wavefield has an integrand $\exp[i\Phi(\mathbf{x}, \mathbf{x}')]$, where $\mathbf{x}$ and $\mathbf{x}'$ are both two dimensional vectors transverse to the LOS. The total phase $\Phi = \phi_g + \phi_r + \phi_d$ comprises a geometric term

$$\phi_g(\mathbf{x}, \mathbf{x}') = \left(\frac{\pi\nu}{c}\right)\left[D_s^{-1}x'^2 + (D - D_s)^{-1}|\mathbf{x} - \mathbf{x}'|^2\right], \tag{B1}$$

a refraction term, ϕ_r, from large-scale variations and the diffraction term, ϕ_d, from small-scale variations. D is the Earth-pulsar distance and D_s is the pulsar-screen distance. In the absence of the refraction term, the scattered wavefield of a point source is described by an ensemble-average image $I_0(\boldsymbol{\theta})$. We include refraction as a quadratic surface centered on a stationary-phase point $\overline{\mathbf{x}}'$ on the screen corresponding to an angle $\overline{\boldsymbol{\theta}}$,

$$\phi_r(\mathbf{x}') = \phi_r(\overline{\mathbf{x}}') + \mathbf{b} \cdot (\mathbf{x}' - \overline{\mathbf{x}}') + (\mathbf{x}' - \overline{\mathbf{x}}') \cdot \mathbf{C} \cdot (\mathbf{x}' - \overline{\mathbf{x}}'). \tag{B2}$$

The stationary phase point is defined with respect to $\phi_g + \phi_r$ and generally there could be multiple stationary phase points. By consolidating linear and quadratic terms, the refraction-distorted image can be written as

$$I(\boldsymbol{\theta}) = I_0(G_x^{-1}(\theta_x - \overline{\theta}_x), G_y^{-1}(\theta_y - \overline{\theta}_y)), \tag{B3}$$

where the gains are given by

$$G_{x,y} = \left[1 + k^{-1}(D_s/D)(D - D_s)C_{x,y}\right]^{-1}. \tag{B4}$$

We assume, for simplicity, that ellipses of constant phase from the last term in Eq. B2 align with the transverse coordinate axes (x, y). In this case, $\mathbf{C}$, is diagonal with elements $C_{x,y}$. A gain $G_{x,y} > 1$ implies that the image is wider in the x, y directions compared to the unity gain case. While the amplitude of the image is unaltered, the integral over the image implies a flux variation by a factor $G_x G_y$. A more general expression that we use in Paper III is

$$I(\boldsymbol{\theta}) = I_0(\mathbf{U}^\dagger \boldsymbol{\gamma_2}^{-1} \mathbf{U}(\boldsymbol{\theta} - \overline{\boldsymbol{\theta}})), \tag{B5}$$

where $\mathbf{U}$ is a 2×2 matrix that diagonalizes $\mathbf{C}$, the dagger denotes transpose, and γ_2 is a diagonal 2×2 matrix with elements G_x^{-1} and G_y^{-1}.

For each point on the screen the time delay relative to the direct ray in vacuum is

$$t = t_{\mathrm{DM}} + \frac{1}{2c}\left[\frac{D(D - D_s)}{D_s}\right]\left[\overline{\theta}^2 + G_x^{-1}(\theta_x - \overline{\theta}_x)^2 + G_y^{-1}(\theta_y - \overline{\theta}_y)^2\right]. \tag{B6}$$

The first term $t_{\mathrm{DM}} = (2\pi\nu)^{-1}\phi_0(\overline{\mathbf{x}}')$ is the extra dispersive delay from the position of the image centroid. The second term is the geometric delay from the centroid of the refracted image. The third term results from the combination of extra geometrical delay and modified dispersive delay from the quadratic part of the refractive phase. A gain $G_x > 1$ requires a converging wavefront that is produced by a deficit of electrons compared to the local mean in the screen. Thus while $G_x > 1$ increases the size of the image in the x direction and increases geometric delays $\propto G_x^2$, these are compensated in part by the reduced dispersion delay.

We average the last term over the distorted image, which we treat as a probability density function with angular variances $(G_x\sigma_{x0})^2$ and $(G_y\sigma_{y0})^2$, yielding

$$t = t_{\mathrm{DM}} + \frac{1}{2c}\left[\frac{D(D - D_s)}{D_s}\right]\left[\overline{\theta}^2 + G_x\sigma_{x0}^2 + G_y\sigma_{y0}^2\right]. \tag{B7}$$

When the undistorted image is symmetric we have $\sigma_{x0} = \sigma_{y0}$ and the time delay then involves a factor that is the the sum of the gains, $G_x + G_y$.

C. FREQUENCY DEPENDENT DISPERSION MEASURE FROM PHASE-SCREEN AVERAGING

Scattered pulsar radiation reaches the Earth from a cone of radius θ_d, the diffraction angle. For simplicity here we assume scattering occurs in a screen a distance $D' = D - D_s$ from the Earth. The screen phase $\phi(\mathbf{x})$ is averaged by the area of the scattering cone $\sim \ell_s^2$ where $\ell_s = D'\theta_d$. DM is related to the screen phase by $\mathrm{DM} = \nu\phi/2\pi a_{\mathrm{DM}}$ where a_{DM} is defined in Eq. 9. The screen-averaged DM is

$$\mathrm{DM}(\nu) = \int d\mathbf{x} \mathrm{W}(\mathbf{x} - \mathbf{x}_0, \nu)\mathrm{DM}(\mathbf{x}), \tag{C1}$$

where the averaging function $W(\mathbf{x})$ has unit area and has a width that is strongly frequency dependent. Letting $\mathbf{x}_0$ be the point on the screen where the direct ray path emerges with an associated dispersion measure $\mathrm{DM}_0 = \mathrm{DM}(\mathbf{x}_0)$, we derive the variance of the difference $\delta\mathrm{DM}(\nu) = \mathrm{DM}(\nu) - \mathrm{DM}_0$. Assuming that the screen phase has stationary statistics, that scattering is circularly symmetric, and assuming that the weighting function has an autocorrelation function $R_W(\mathbf{x}, \mathbf{x}', \nu)$ that depends only on the difference $\mathbf{x} - \mathbf{x}'$, we can write the DM variations in terms of the phase structure function $D_\phi(\delta\mathbf{x})$

$$\left\langle [\delta\mathrm{DM}(\nu)]^2 \right\rangle = \frac{1}{2\pi} \left(\frac{\nu}{a_{\mathrm{DM}}} \right)^2 \int dy \, y \, D_\phi(y) \left[W(y, \nu) - \frac{1}{2} R_W(y, \nu) \right]. \tag{C2}$$

If we use the Kolmogorov form $D_\phi(y) \propto y^{5/3}$ (see main text and Cordes & Lazio (1991); Cordes & Rickett (1998)) and if we approximate the weighting function as ℓ_s^{-2} that drops to zero at a radius ℓ_s, we obtain

$$\left\langle [\delta\mathrm{DM}(\nu)]^2 \right\rangle = \frac{3 f_{5/3}}{22\pi^2} \left(\frac{r_e c}{a_{\mathrm{DM}}} \right)^2 \mathrm{SM}\ell_s^{5/3}. \tag{C3}$$

Using $\ell_s = D' \theta_d$ and the relation for a Kolmogorov medium in strong scattering (Cordes & Lazio 1991, 2002)

$$\theta_d = 0.071 \text{ arc sec } \mathrm{SM}^{3/5} \nu^{-11/5}, \tag{C4}$$

we obtain

$$\left\langle [\delta\mathrm{DM}(\nu)]^2 \right\rangle^{1/2} \approx 10^{-1.05} \text{ pc cm}^{-3} \, \mathrm{SM}D'^{5/5} \nu^{-11/6}. \tag{C5}$$

The associated rms time delay is

$$\Delta t_{\delta\mathrm{DM}} = 4.15 \times 10^{-3} \, s \, \nu^{-2} \left\langle [\delta\mathrm{DM}(\nu)]^2 \right\rangle^{1/2} \approx 0.118 \, \mu s D'^{5/6} \nu^{-23/16} \left(\frac{\mathrm{SM}}{10^{-3.5}} \text{ kpc m}^{-20/3} \right). \tag{C6}$$

D. LEAST-SQUARES FITTING OF MULTIFREQUENCY DATA

Consider a set of multi-frequency TOA measurements obtained in an observing session at a given epoch, $\{t_k, \nu_k, k = 1, n_\nu\}$. We model the TOAs as $t(\nu) = t_\infty + t_{\mathrm{DM}}(\nu) + t_C(\nu) + \epsilon(\nu)$ where t_∞ is the TOA at infinite frequency, t_{DM} is the delay from plasma dispersion, t_C is an additional, non-dispersive chromatic perturbation (e.g. from scattering), and ϵ is measurement error that we consider to be white noise (statistically independent). Actually, t_C is the sum of several effects as outlined in the main text, but for convenience here we use only one term. In vector form the TOAs are $\mathbf{D} = \mathbf{X}\boldsymbol{\theta} + \boldsymbol{\epsilon}$, where $\mathbf{D} = \mathrm{col}\{t_k\}$ is a column vector of arrival times, $\boldsymbol{\theta}$ is a vector of parameters, and $\mathbf{X}$ comprises the independent variables. With frequency-dependent errors described by a covariance matrix $\mathbf{C}$, the solution is $\boldsymbol{\theta} = \left(\mathbf{X}^\dagger \mathbf{C}^{-1} \mathbf{X} \right)^{-1} \mathbf{X}^\dagger \mathbf{C}^{-1} \mathbf{D}$. The covariance matrix for parameter errors is $\mathbf{P} = \left(\mathbf{X}^\dagger \mathbf{C}^{-1} \mathbf{X} \right)^{-1}$ if the model is correct (only additive errors to the TOAs). For white-noise errors in TOAs at the different frequencies, $\mathbf{C} = \mathrm{diagonal}\left\{ \sigma_k^2 \right\}$. In the following we will use the quantities

$$r_p \equiv \sum_k \sigma_k^{-2} \nu_k^{-p} \ln \nu_k, \qquad s_p \equiv \sum_k \sigma_k^{-2} \nu_k^{-p}. \tag{D1}$$

If we fit only for t_∞ and there are no chromatic effects (the situation at very high radio frequencies and in high-energy observations) the variance is $\sigma_{t_\infty}^2 = 1/s_0$. When the errors are identical at all frequencies, $\sigma_{t_\infty}^2 = \sigma^2/n_\nu$.

Fit for dispersion: Consider a two-parameter fit that includes the dispersion term along with t_∞ and that there are no other chromatic effects in the data. The parameter vector is $\boldsymbol{\theta} = \mathrm{col}\left(t_\infty, a_{\mathrm{DM}}\mathrm{DM} \right)$, the variables matrix is $\mathbf{X} = \mathrm{matrix}(1 \ \nu_i^{-2})$, $i = 1, \ldots, n_\nu$, and the standard errors are $\sigma_{t_\infty}^2 = s_4/\mathcal{D}_2$ for t_∞ and $\sigma_{\mathrm{DM}}^2 = s_0/a_{\mathrm{DM}}^2 \mathcal{D}_2$ for DM, where $\mathcal{D}_2 = s_0 s_4 - s_2^2$ is the determinant of $\mathbf{X}^\dagger \mathbf{C}^{-1} \mathbf{X}$.

An alternative approach uses an ancillary value of DM (e.g. interpolated from measurements at other epochs) that will have an error $\delta\mathrm{DM}$. The TOA error is then $\sigma_{t_\infty}^2 = s_0^{-1} + (a_{\mathrm{DM}}\delta\mathrm{DM}s_2/s_0)^2$, which is better than the two-parameter fit if $\delta\mathrm{DM} < a_{\mathrm{DM}}^{-1} \left(s_0/\mathcal{D}_2 \right)^{1/2}$ Evaluating in the continuous limit with errors that are independent of frequency and letting $\nu_2 = \nu_1 - B$ where B is the total bandwidth and $\sigma_B = \sigma/\sqrt{n_\nu}$, we require

$$\delta\mathrm{DM} < \frac{\sigma_B}{a_{\mathrm{DM}}} \frac{\sqrt{3}\nu_1^3}{B} (1 - B/\nu_1)^{3/2} = 10^{-3.38} \text{ pc cm}^{-3} \frac{\nu_1^3}{B} (1 - B/\nu_1)^{3/2} \sigma_B(\mu s) \tag{D2}$$

for ν_1 and B in GHz.

Now consider the case where the data contain the chromatic term $t_C(\nu)$ but the fitting function does not. If $t_C(\nu)$ is deterministic[3] the additional, systematic errors are

$$\delta t_\infty = \mathcal{D}_2^{-1} \sum_k \sigma_k^{-2}(s_4 - s_2\nu_k^{-2})t_C(\nu_k) = -a_C R_{t_\infty} = a_C \mathcal{D}_2^{-1}\left(s_4 s_X - s_2 s_{X+2}\right) \tag{D3}$$

$$\delta\mathrm{DM} = \mathcal{D}_2^{-1} \sum_k \sigma_k^{-2}(s_0\nu_k^{-2} - s_2)t_C(\nu_k) = a_C\left(a_{\mathrm{DM}}\mathcal{D}_2\right)^{-1}\left(s_0 s_{X+2} - s_2 s_X\right) \tag{D4}$$

where the last equality in each equation holds for a power law scaling, $t_C(\nu) = a_c\nu^{-X}$. Because it absorbs some of the scattering delay, t_C, $\delta\mathrm{DM}$ is always positive, causing TOAs to be overcorrected and producing a negative bias in t_∞.

A simple case is where narrowband measurements are made at two frequencies $\nu_{1,2}$ with $r = \nu_1/\nu_2$. The error from the chromatic term is $\delta t_\infty = \left(r^2 t_{C_1} - t_{C_2}\right)/\left(r^2 - 1\right)$. For an octave bandwidth ($r = 2$), the TOA error is approximately $-1/3$ of the chromatic term at the lower frequency when $\nu_1 \gg \nu_2$ so that $t_{C_2} \gg t_{C_1}$. Not surprisingly, observations over an octave at low frequencies where t_C is larger will be substantially worse than at high frequencies. For large r we have $\delta t_\infty \approx -r^{X-2}t_{C_1}$, showing that the chromatic term at the higher frequency is amplified by a large factor when $X = 4$.

For $n_\nu = 1024$, $\nu_1 = 2$ GHz and $\nu_1 = 1$ GHz, we get $\delta t_\infty/a_c = -0.29$ and $\delta\mathrm{DMa}_{\mathrm{DM}}/a_C = 1.15$. Suppose that $a_C = 1$ μs if all frequencies are expressed in GHz, equivalent to $t_C(1\text{ GHz}) = 1$ μs. In this case $\delta t_\infty = -0.29$ μs and $\delta\mathrm{DM} = (1.15\ \mu s/4.15\text{ ms})\text{pc cm}^{-3} = 10^{-3.62}$ pc cm^{-3}. It may be more convenient to express the systematic errors in terms of t_C at either the highest or lowest frequency, in which case the relations $a_C = t_C\nu_1^X = t_C\nu_2^X$ can be used.

Various trends can be identified by considering other cases. For fixed total bandwidth B, the systematic TOA error decreases with increasing upper frequency ν_1. For fixed upper frequency, the *systematic error* increases as B gets larger (i.e. as the lower frequency gets lower). Counteracting this trend is the decrease in *standard error* with larger bandwidth, implying that there is an optimal bandwidth that depends on the pulsar spectrum and system noise vs. frequency along with the scattering strength.

Fit for dispersion and scattering: Now we include scattering as a single term in the fitting function, $t_C(\nu) = a_C\nu^{-X}$, and assume initially that the exponent X is known. Then $\boldsymbol{\theta} = \mathrm{col}\,(t_\infty, a_{\mathrm{DM}}\mathrm{DM}, a_C)$ and the variables matrix is $\mathbf{X} = \mathrm{matrix}(1\ \ \nu_i^{-2}\ \ \nu_i^{-X})$, $i = 1, \ldots, n_\nu$.

When X is assumed to be X_0, the error $\delta X = X_0 - X$, causes a systematic error from an extra term obtained from the expansion, $t_C(\nu; X_0) \approx a_C\nu^{-X} - a_C\delta X\nu^{-X}\ln\nu$. The error on the arrival time to linear order in δX is

$$\delta t_\infty = -a_C\delta X G_{t_\infty} \tag{D5}$$

where

$$G_{t_\infty} = \mathcal{D}_3^{-1}\left[r_X\left(s_4 s_{2X} - s_{X+2}^2\right)r_{X+2}\left(s_X s_{X+2} - s_2 s_{2X}\right) + r_{2X}\left(s_2 s_{X+2} - s_4 s_X\right)\right] \tag{D6}$$

and

$$\mathcal{D}_3 = \det \mathbf{X}^\dagger\mathbf{C}^{-1}\mathbf{X} = (s_0 s_4 - s_2^2)s_{2X} + 2s_2 s_X s_{X+2} - (s_4 s_X^2 + s_0 s_{X+2}^2). \tag{D7}$$

Evaluting for the same case as above with $n_\nu = 1024$, $\nu_1 = 2$ GHz and $\nu_2 = 1$ GHz, we obtain $G_{t_\infty} = -0.069$ implying for $\delta X > 0$ that, opposite to before, the TOA is underrcorrected because DM is biased low while the scattering parameter a_C is biased high. When $\delta X < 0$ the opposite is true. Either way, the amplitude of the timing error is small, $\delta t_\infty = 0.069 a_C\delta X$.

Finally, a four parameter fit can include δX in an iterative approach that uses an initial value for X and interates. The parameter vector is $\boldsymbol{\theta} = \mathrm{col}\,(t_\infty, a_{\mathrm{DM}}\mathrm{DM}, a_C, a_{C_0}\delta X)$ and the variables matrix is $\mathbf{X} = \mathrm{matrix}(1\ \ \nu_i^{-2}\ \ \nu_i^{-X}\ \ -a_{C_0}\nu_i^{-X_0}\ln\nu_i)$, $i = 1, \ldots, n_\nu$. In this case, initial choices for a_{C_0} and X_0 are updated by fitted values for a_C and δX.

---

[3]
  Stochastic t_C will yield an error in t_∞ that involves the correlation function $\langle t_C(\nu)t_C(\nu')\rangle$, but we will not elaborate on this case in this paper.

REFERENCES

Anholm, M. et al. 2009, Phys. Rev. D, 79, 084030
Armstrong, J. W. 1984, Nature, 307, 527
Armstrong, J. W., Rickett, B. J., & Spangler, S. R. 1995, ApJ, 443, 209
Ahuja, A. L., Mitra, D., & Gupta, Y. 2007, MNRAS, 377, 677
Backer, D. C. et al. 1982, Nature, 300, 615
Backer, D. C., & Hellings, R. W. 1986, ARA&A, 24, 537
Backer, D. C. et al. 1993, ApJ, 404, 636
Bailes, M. 2007, arXiv:astro-ph/0702698
Barnard, J. J., & Arons, J. 1986, ApJ, 302, 138
Bertotti, B., Carr, B. J., & Rees, M. J. 1983, MNRAS, 203, 945
Bhat, N. D. R., Cordes, J. M., & Chatterjee, S. 2003, ApJ, 584, 782
Bhat, N. D. R. et al. 2004, ApJ, 605, 759
Brisken, W. F. et al. 2010, ApJ, 708, 232
Britton, M. C. 2000, ApJ, 532, 1240
Cognard, I., & Lestrade, J.-F. 1997, A&A, 323, 211
Coles, W. A. et al. 2010, ApJ, 717, 1206
Cordes, J. M. 1993, Planets Around Pulsars, 36, 43
Cordes, J. M., Weisberg, J. M., & Boriakoff, V. 1985, ApJ, 288, 221
Cordes, J. M. & Downs, G. S. 1985, ApJS, 59, 343
Cordes, J. M., & Stinebring, D. R. 1984, ApJ, 277, L53
Cordes, J. M., Pidwerbetsky, A., & Lovelace, R. V. E. 1986, ApJ, 310, 737
Cordes, J. M. et al. 1990, ApJ, 349, 245
Cordes, J. M., & Lazio, T. J. 1991, ApJ, 376, 123
Cordes, J. M. & Rickett, B. J. ApJ, 507, 846
Cordes, J. M. & Lazio, T.J.W. 2001, ApJ, 549, 997
Cordes, J. M., & Lazio, T. J. W. 2002, arXiv:astro-ph/0207156
Cordes, J. M. et al. 2004, ApJ, 612, 375
Cordes, J. M. et al. 2004, New Astronomy Review, 48, 1413
Cordes, J. M. et al. 2006, ApJ, 637, 346
Cortés Medellín, G. 2007, SKA Memo 95, "Antenna Noise Temperature Calculation," http://www.skatelescope.org/
Craft, H. D., Jr. 1970, Ph.D. Thesis
Damour, T., & Vilenkin, A. 2005, Phys. Rev. D, 71, 063510
Deneva, J. S., Cordes, J. M., & Lazio, T. J. W. 2009, ApJ, 702, L177
D'Alessandro, F., McCulloch, P. M., King, E. A., Hamilton, P. A., & McConnell, D. 1993, MNRAS, 261, 883
Demorest, P. B. 2007, Ph.D. Thesis, U.C. Berkeley.
Desai, K. M., & Fey, A. L. 2001, ApJS, 133, 395
Detweiler, S. 1979, ApJ, 234, 1100
Downs, G. S., & Reichley, P. E. 1983, ApJS, 53, 169
Edwards, R. T. & Stappers, B. W. 2003, å, 407, 273
Edwards, R. T., Hobbs, G. B., & Manchester, R. N. 2006, MNRAS, 372, 1549
Finn, L. S., & Lommen, A. N. 2010, arXiv:1004.3499
Foster, R. S., & Backer, D. C. 1990, ApJ, 361, 300
Foster, R. S., & Cordes, J. M. 1990, ApJ, 364, 123
Freire, P. C. et al. 2009, arXiv:0902.2891
Haslam, C. G. T. et al. 1982, A&AS, 47, 1
Helfand, D. J., Manchester, R. N., & Taylor, J. H. 1975, ApJ, 198, 661
Hellings, R. W., & Downs, G. S. 1983, ApJ, 265, L39
Hemberger, D. A., & Stinebring, D. R. 2008, ApJ, 674, L37
Hill, A. S. et al. 2003, ApJ, 599, 457
Hill, A. S. et al. 2005, ApJ, 619, L171
Hobbs, G. B., et al. 2009, Publications of the Astronomical Society of Australia, 26, 103

Hobbs, G., et al. 2010, Classical and Quantum Gravity, 27, 084013
Hotan, A. W., Bailes, M., & Ord, S. M. 2006, MNRAS, 369, 1502
Hu, W., Stinebring, D. R., & Romani, R. W. 1991, ApJ, 366, L33
Jacoby, B. A. 2005, ApJ, 629, L113
Jaffe, A. H., & Backer, D. C. 2003, ApJ, 583, 616
Jenet, F. A. et al. 1998, ApJ, 498, 365
Jenet, F. A., Anderson, S. B., & Prince, T. A. 2001, ApJ, 546, 394
Jenet, F. A., & Gil, J. 2004, ApJ, 602, L89
Jenet, F. A. et al. 2004, ApJ, 606, 799
Jenet, F. A. et al. 2005, Binary Radio Pulsars, 328, 399
Jenet, F. A. et al. 2005, ApJ, 625, L123
Jenet, F. A. et al. 2006, ApJ, 653, 1571
Jenet, F. A. et al. 2009, arXiv:0909.1058
Kaspi, V. M., Taylor, J. H., & Ryba, M. F. 1994, ApJ, 428, 713
Kinkhabwala, A., & Thorsett, S. E. 2000, ApJ, 535, 365
Kramer, M. et al. 2004, New Astronomy Review, 48, 993
Kramer, M., et al. 2006, Science, 314, 97
Kuz'min, A. D., & Izvekova, V. A. 1993, MNRAS, 260, 724
Lambert, H. C. & Rickett, B. J. 1999, ApJ, 517, 299
Lambert, H. C. & Rickett, B. J. 2000, ApJ, 531, 883
Lazio, T. J. W. 2004, ApJ, 613, 1023
Lee, K. J., Jenet, F. A., & Price, R. H. 2008, ApJ, 685, 1304
Löhmer, O. et al. 2001, ApJ, 562, L157
Löhmer, O. et al. 2004, A&A, 425, 569
Lorimer, D. R. et al. 1995, MNRAS, 273, 411
Lundgren, S. C. et al. 1995, ApJ, 453, 433
Lyne, A. G. 2010, Science, 329, 408
Manchester, R. N. et al. 2005, AJ, 129, 1993
McLaughlin, M. A. et al. 2002, ApJ, 564, 333
Mitra, D., & Rankin, J. M. 2002, ApJ, 577, 322
Narayan, R., & Goodman, J. 1989, MNRAS, 238, 963
Phillips, J. A., & Wolszczan, A. 1991, ApJ, 382, L27
Pshirkov, M. S., & Tuntsov, A. V. 2010, Phys. Rev. D, 81, 083519
Ramachandran, R. et al. 2006, ApJ, 645, 303
Rathnasree, N., & Rankin, J. M. 1995, ApJ, 452, 814
Rickett, B. J. 1990, ARA&A, 28, 56
Rickett, B. et al. 2009, MNRAS, 395, 1391
Romani, R. W., & Taylor, J. H. 1983, ApJ, 265, L35
Romani, R. W., Narayan, R., & Blandford, R. 1986, MNRAS, 220, 19
Ruderman, M. & Sutherland, P. 1975, ApJ, 196, 51
Sallmen, S. et al. 1999, ApJ, 517, 460
Scargle, J. D. 1981, ApJS, 45, 1
Sesana, A., & Vecchio, A. 2010, Classical and Quantum Gravity, 27, 084016
Seto, N., & Cooray, A. 2007, ApJ, 659, L33
Shannon, R. & Cordes, J. M. 2010, ApJ, submitted
Spangler, S. R., & Gwinn, C. R. 1990, ApJ, 353, L29
Stinebring, D. R. et al. 1990, Physical Review Letters, 65, 285
Stinebring, D. R. et al. 2001, ApJ, 549, L97
Tanenbaum, B. S., Zeissig, G. A., & Drake, F. D. 1968, Science, 160, 760
Taylor, J. H., & Weisberg, J. M. 1982, ApJ, 253, 908
van Haasteren et al. 2009, MNRAS, 395, 1005
van Straten, W. 2009, ApJ, 694, 1413
Verbiest, J. P. W., et al. 2009, MNRAS, 400, 951
Walker, M. A. et al. 2008, MNRAS, 388, 1214
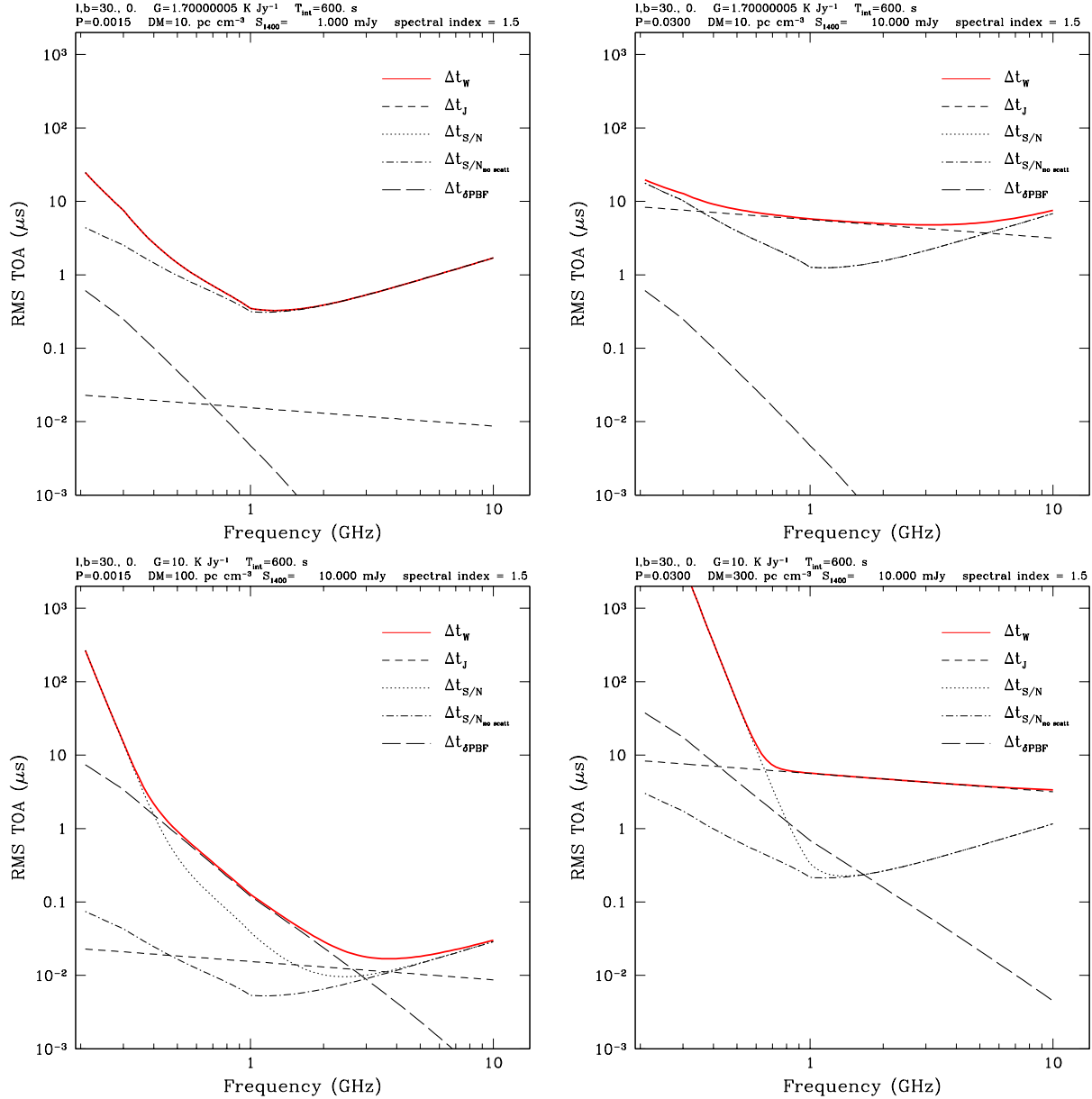You, X. P., et al. 2007, MNRAS, 378, 493

FIG. 6.— Rms timing errors that contribute to the white-noise term in Eq. 29 are shown plotted against frequency. The top two curves are calculated for a 100-m class (GBT-like) telescope with gain $G = 1.7$ K Jy^{-1} while the bottom curves are for an Arecibo-like telescope with large gain, $G = 10$ K Jy^{-1}. Flux densities quoted below are for 1.4 GHz and scale with frequency as $\nu^{-1.5}$. The bandwidth ratio B/ν is 0.05 for frequencies below 0.3 GHz, increases linearly to 0.2 from 0.3 to 1 GHz, and stays at 0.2 for higher frequencies. Solid (red) curves: the total white-noise contribution to the TOA error. Dot-dash curves: $\Delta t_{S/N}$ calculated using the intrinsic pulse width; these are underestimates of the true TOA error from radiometer noise. Radiometer noise includes a constant temperature added to the 408 MHz background temperature from (Haslam et al. 1982). The intrinsic pulse shape is Gaussian in form with a duty cycle of 0.03 at 1.4 GHz that scales as $\nu^{-0.2}$. The duty cycle also scales with spin period as $P^{-0.4}$ for periods longer than 2 ms but are allowed to be small (0.02) for shorter periods to model those MSPs with very narrow pulses. The pulse width used to calculate the contribution from radiometer noise ($\Delta t_{S/N}$) includes the effects of interstellar pulse broadening calculated using the NE2001 electron-density model. Dotted curves: the radiometer-noise timing error ($\Delta t_{S/N}$) calculated using the apparent pulse width that includes interstellar scattering broadening; Short-dashed curves: The contribution from pulse-phase-jitter (Δt_J) using a jitter parameter $f_J = 1/3$. Long-dashed curves: Timing errors from the finite number of scintles ($\Delta t_{\delta PBF}$). The scintillation time used to calculate $\Delta t_{\delta PBF}$ is based on a fiducial transverse velocity of 100 km s^{-1}. (Top left:) Millisecond pulsar ($P = 1.5$ ms) that is nearby with DM=10 cm^{-3}; the TOA is noise limited because the flux density (1 mJy) and the telescope gain (1.7 K Jy^{-1}) are low. (Top right:) 30-ms pulsar that is nearby but bright enough that its timing is jitter dominated for most of the frequency range. (Bottom left:) Millisecond pulsar with moderate DM = 100 pc cm^{-3} and high enough flux density (10 mJy) observed with high gain (10 K Jy^{-1}) so that the timing is dominated by the DISS finite-scintle effect. (Bottom right:) 30-ms pulsar with large DM (300 pc cm^{-3} and large flux density (10 mJy) observed with high gain such that the timing errors are jitter dominated at high frequencies but are noise limited at low frequencies owing to pulse broadening from interstellar scattering.
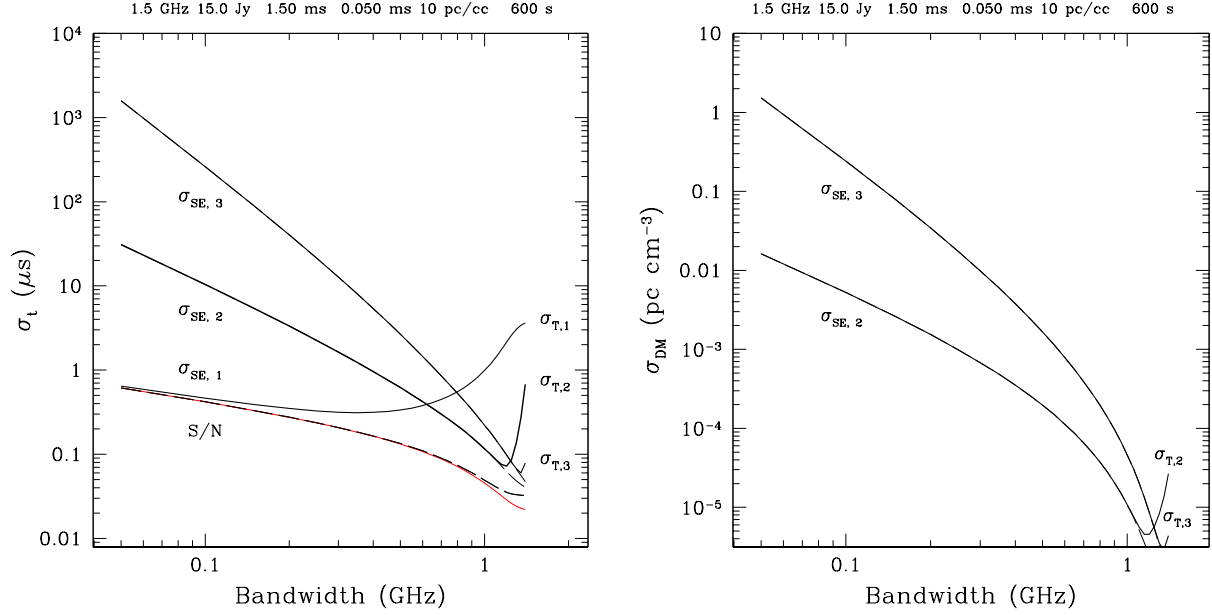
FIG. 7.— Left: Standard and systematic errors after fitting multifrequency TOAs across the designated bandwidth with a maximum frequency of 1.5 GHz. These errors apply to cases where the only chromatic terms included are the dispersive term t_{DM} and an additional term $t_C \propto \nu^{-X}$ with $X = 4.4$ that approximates pulse broadening or one of the refraction terms discussed in the text. The curves apply to a 600 s observation using a 100-m class telescope of a pulsar with $P = 1.5$ ms and DM $= 10$ pc cm^{-3} in the direction $\ell = 45°$, $b = 0°$. The pulse width is 50 μs. Dashed lines labeled $\sigma_{\mathrm{SE},k}$, $k = 1, 2, 3$ are the standard errors for one, two and three-parameter fits as discussed in the text. Solid lines labeled $\sigma_{t,k}$ are total errors that quadratically sum standard and systematic errors. For $k = 1$, the systematic error includes an error in dispersion measure, $\delta\mathrm{DM} = 10^{-3.5}$ pc cm^{-3} along with pulse broadening calculated using NE2001. For $k = 2$, the systematic error is solely from pulse broadening because DM is fitted for. For $k = 3$, an error $\delta X = 0.44$ (10 %) is assumed in the exponent of the pulse-broadening scaling law. The curve labeled "S/N" is the standard error resulting solely from radiometer noise. It scales as $B^{-1/2}$ for small bandwidths but steepens as larger bandwidths include frequencies where the flux density is higher. The difference between the total error and the standard error for the two-parameter fit is caused by the scattering term, t_C. This example shows that a 3-parameter fit can remove much of the scattering when large bandwidths are used, allowing pulsars with large DMs to be included in a pulsar timing array Right: Similar plots for errors in DM when it is included in two and three-parameter fits.

2 GHz 15.0 Jy 1.50 ms 0.050 ms 30 pc/cc 600 s

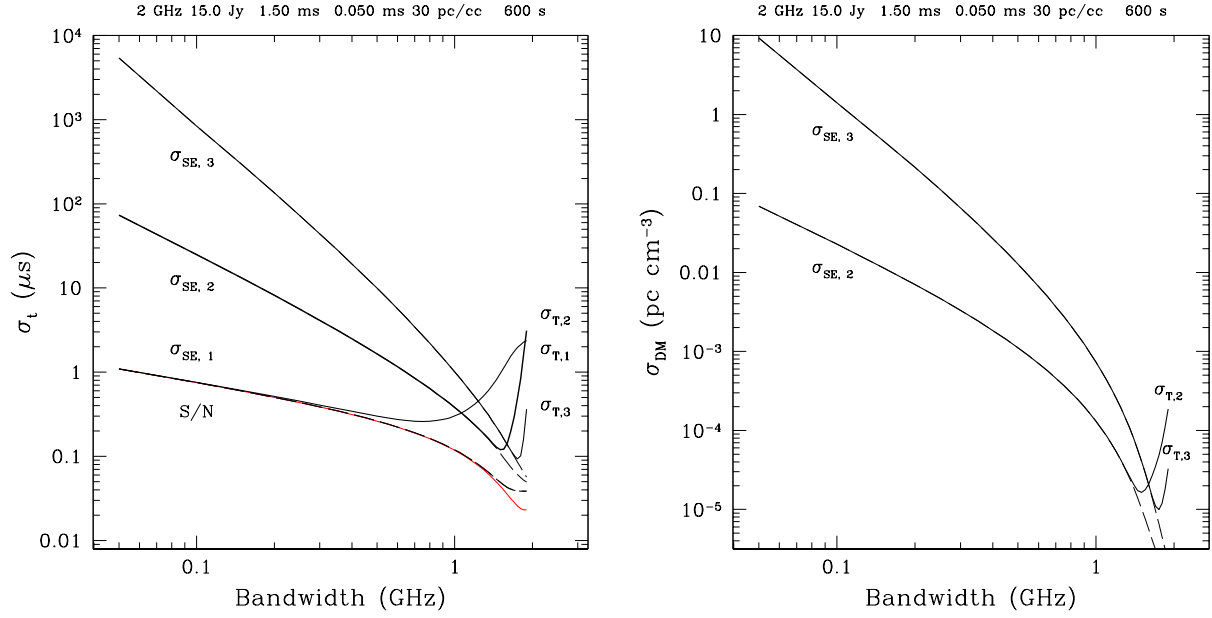2 GHz 15.0 Jy 1.50 ms 0.050 ms 30 pc/cc 600 s

FIG. 8.— Plot of standard and systematic errors for multifrequency fits to arrival times in the same format and for the same pulsar parameters as in Figure 7 except for a dispersion measure DM = 100 pc cm^{-3} and a maximum frequency of 2 GHz. The left-hand panel is for a 100-m class telescope with $S_{sys} = 15$ Jy and the right-hand panel is for an Arecibo-class telescope with $S_{sys} = 4$ Jy.

1.5 GHz 15.0 Jy 1.50 ms 0.050 ms 10 pc/cc 600 s

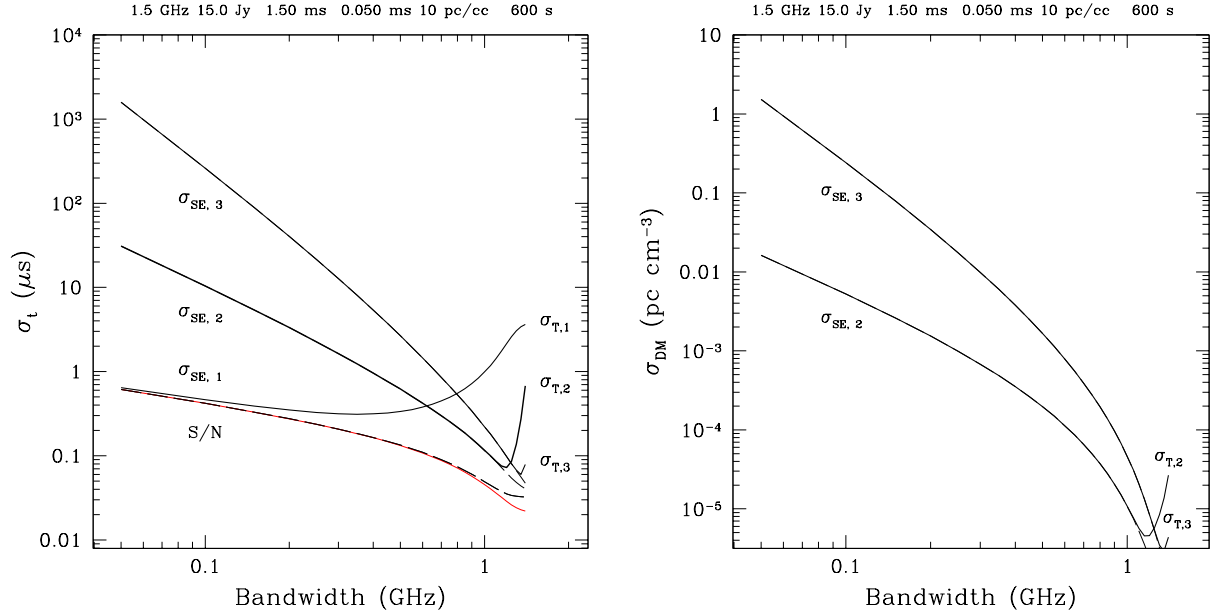1.5 GHz 15.0 Jy 1.50 ms 0.050 ms 10 pc/cc 600 s

FIG. 9.— Plot of standard and systematic errors for multifrequency fits to arrival times in the same format and for the same pulsar parameters as in Figure 7 except for a dispersion measure DM = 500 pc cm^{-3} and an upper frequency of 5 GHz. The left-hand panel is for a an Arecibo-class telescope with $S_{sys} = 4$ Jy) and the right-hand panel is for the full SKA with $S_{sys} = 0.3$ Jy.